D2.3 Crushed Li-ore characterization (TUBAF) 29/08/2025

Author: Dr. Asija Durjagina
Entity: TECHNISCHE UNIVERSITAET BERGAKADEMIE FREIBERG (TUBAF)

Funded by the European Union

Funded by the European Union. Views and opinions expressed are however those of the author(s) only and do not necessarily reflect those of the European Union or the European Climate, Infrastructure and Environment Executive Agency (CINEA). Neither the European Union nor CINEA can be held responsible for them.

DOCUMENT CONTROL SHEET

Project	**Li4LIFE** – NOVEL DOMESTIC BATTERY GRADE LITHIUM CARBONATE VALUE CHAIN FOR GREEN LIFE

General information				
Work Package	2			
Deliverable Number and name	2.3 Crushed Li-Ore Characterization			
Due Date	29/08/2025			
Submission Date				
Deliverable Lead organisation	TECHNISCHE UNIVERSITAET BERGAKADEMIE FREIBERG (TUBAF)			
Dissemination Level		Public (PU)	x	Confidential (CO)
Document Nature	x	Report (R)		Other (O)
Description of the related task and the deliverable. (Extract from DoA)	Task 2.3: Mineralogical and geochemical characterisation of the selected lithium bearing minerals Detailed mineralogical and geochemical analyses (automated mineralogy, LA-ICP-MS, LIBS, elemental imaging/ mapping) will be conducted on selected lithium-bearing minerals and ore samples in order to assay Li content in both main ores as well as from rock-forming minerals. Such characterisation will investigate the Li ore samples in a complex way, looking also for the other rock/mineral properties, possible by-products (with focus on CRM or strategic raw materials for the EU) or detection of impurities that may have serious impact on the effectivity and/or economics of the beneficiation process. All information will be continuously shared among project partners; the final report will summarise data of all Li-ore samples from both major and additional localities (D2.6 at M30). The ore parameters characteristics will be also studied on crushed samples. The crushed samples will be characterized from sieved fractions. The results will be summarised in an early report (D2.3 at M18). The mineralogical study includes especially the following items: (1) Preparation of polished sections from each size fraction; (2) Mineralogical study of the sections using the QMA technique (3) Chemical composition of the main ore minerals			
Authors	Dr. Asija Durjagina (TUBAF)			
Reviewers	Jan Cempirek (MUNI), Vojtech Werticj (MUNI)			
Status		Draft	x	Final

Revision History				
Version	Date	Reviewer	Organisation	Status
V1	01/09/2025	MM, AD	TUBAF	First draft
V2	22/09/2025	VW, JC	MUNI	Second draft
V3	17/10/2025	MM, AD	TUBAF	Third draft
V4	20/10/2025	MM, AR	ICAMCYL	Final draft

INDEX

LIST OF FIGURES

LIST OF TABLES

EXECUTIVE SUMMARY

This deliverable presents the results obtained in mineralogical and petrophysical investigations. These investigations are used to obtain the rocks characteristics. A summary of the current status of the work associated with each ore is presented below:

- Li rich montmorillonite clays, Swinefordite (Valjevo, Serbia): The original sample was received, but the sample amount was not sufficient to perform mineralogical and petrophysical investigations; therefore, it is not included in the report.
- Lepidolite (Villasrubias pegmatite, Castile and Leon, Spain): The original sample was received, and mineralogical and petrophysical investigations were performed (QMA, VHT, PLT, chemical analysis).
- Zinnwaldite (Cínovec, Czech Republic): The original sample was received, and mineralogical and petrophysical investigations were performed (QMA, VHT, PLT, chemical analysis).
- Petalite (Presqueira pegmatite, Galicia, Spain): The original sample was received with a delay, preliminary mineralogical and petrophysical investigations were performed (microscopic analysis, VHT, PLT).

This report will focus mainly on the lepidolite and zinnwaldite ores, as most complete set of mineralogical and petrophysical investigations have been performed on them. This report will be updated at the end of 2025.

ABBREVIATIONS AND ACRONYMS

Glossary	
Acronym	**Meaning**
QMA	Quantitative mineralogical analysis
VHT	Vickers hardness test
UCT	Uniaxial compression test
PLT	Point Load Test
ICP-OES	Inductively coupled plasma optical emission spectroscopy
LND	Logarithmic normal distribution
CIZ	Central Iberian Zone
LCT	Lithium–cesium–tantalum
CEG	Schist–Greywacke Complex
REM	Raster-electron analysis
MLA	Mineral liberation analysis
LEFM	Linear elastic fracture mechanics
ISRM	International Society for Rock Mechanics and Rock Engineering

Mineralogical and geochemical characterisation of selected lithium-bearing minerals

1. Mathematical-petrographic rock analyses

Rock names are not suitable as synonyms for rock properties in petrophysical modelling as the petrographic description of a rock is based primarily on its genetic, mineralogical and chemical classification criteria whereas aspects related to the rock fabric are only taken into account as a secondary factor.
One alternative is a formal characterization of the rocks. The values of this characterization are neutral, that is determined independently from the application, and are interpreted for application in a specific case. To use a formal characterization of the rocks for technology-related purposes, this must be accessible and describable in mathematical terms. A further requirement is that this characterization is based on geological working methods and terms. Mathematical-petrographic rock characterization can quantitatively describe both the mineral composition as well as the structural constitution of the most important rock types.

General information on describing the fabric of a rock

A rock can be described based on the content of its mineral components and its fabric. A hard rock, for example, consists of the individual mineral phases, but also contains defects (e.g. pores, cracks), which form the continuous phases (gas or liquid phase) and glasses as well as cryptocrystalline masses which are combined to a non-differentiated phase. Each single constituent of a phase – also termed microbody – takes up a certain volume that is defined by boundary surfaces. The term "rock fabric" can be understood as the quantity of all geometric data of a piece of rock. The fabric of a rock comprises its texture and structure.
The texture of a rock is the term used to describe the nature of its composition of individual components. The texture is dictated by the form of the individual mineral components and their mutual geometric relationships. Accordingly, the grain shapes and the grain sizes of the mineral components are essential elements of the rock texture.
The structure of a rock depends on the spatial arrangement of its components. In this case, the components are less the individual grains and far more complexes of the same minerals or other identical structural elements. In this context, the orientation of the components as the directional texture, the distribution of the same as the distribution texture and relative density (compact and porous rocks) are taken into consideration. Rocks with strata of varying mineral composition therefore have

an inhomogeneous distribution texture; lava with gas bubbles is characterized by the special nature of its incomplete relative density.
To apply the characteristics of the rock fabric in technology, the texture must be expressed in figures. For this purpose, stereological methods are applied (Popov, 2007). The characteristics of the rock fabric quantified with the help of these methods are based on the formal characterization of the rocks by geologists. This procedure was selected to make the geometric characteristics determined clear and facilitate under-standing between geologists and engineers with their respective terminology. On the basis of the rock analysis and its mathematical formulation, rock characteristics can now be calculated in the form of characteristic values oriented to the terminology of the geologist.
Based on the application of stereological methods, the rock is quantitatively described by means of its *mode* (content of the individual mineral phases in the rock fabric) characteristic values for the *texture* (e.g. grain size and shape, intergrowth) as well as characteristic values for the *structure* (e.g. direction, distribution and relative density). The basic procedure for a stereological rock test QMA (Quantitative mineralogical analysis) is described by Popov (2007). After proper removal of a defined number of rock samples from the deposit, three ground sections perpendicular to each other were prepared from each rock specimen, which were classified in a library of thin sections (Figure 1).

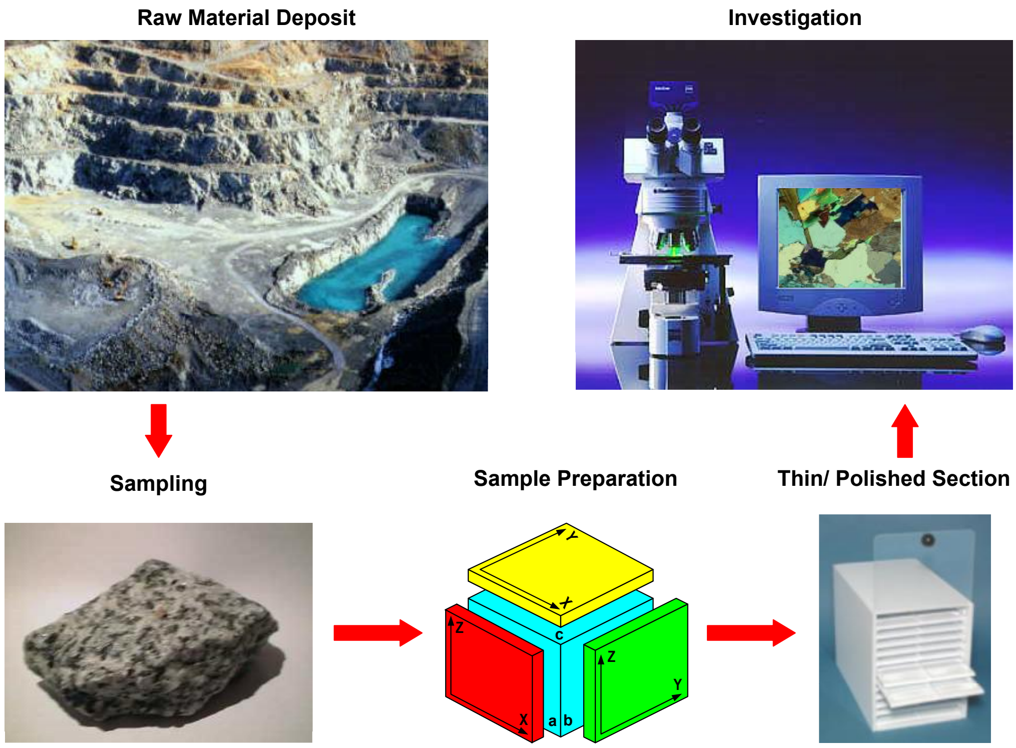

Figure 1 Raw material investigation

These sections were then evaluated with the help of a polarization microscope. The thin section images were assessed by means of various stereological methods (Figure 2).

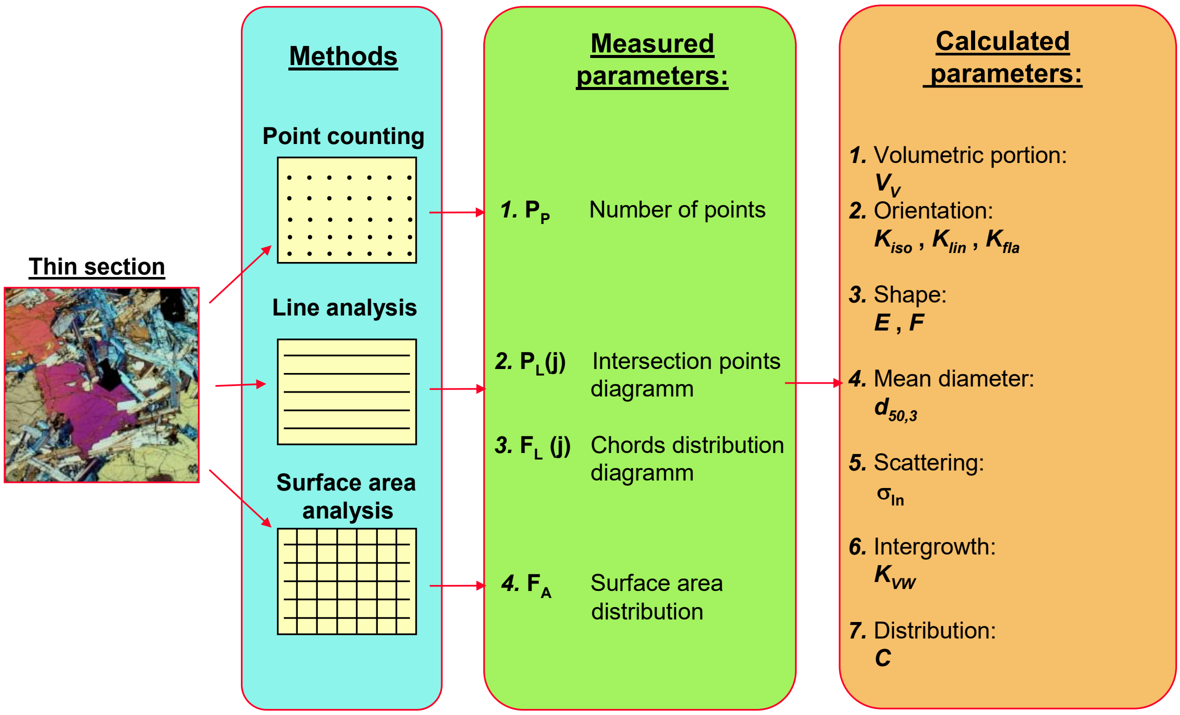

Figure 2 Methods of QMA

With the help of a mathematical model developed at the Institute of Mineral Processing Machines, the rocks were quantitatively characterized based on the calculation of relevant structural and textural characteristic data (Figure 3**¡Error! No se encuentra el origen de la referencia.**). In the following report, the most important characteristic values are explained in greater detail:

Mode (volume percentage of the mineral phases)

The volume percentages of the phases in the rock fabric were determined based on the images of the three mutually perpendicular polished sections. The determination of the point percentage of a phase with the help of a dot matrix superimposed on the images and the arithmetic mean of the point percentages from the three polished planes results in the volume percentage of a phase.

Texture

Particle size of the minerals. The individual microbodies are polydispersed in the rock fabric so that the size of the microbodies must be approximated with a size distribution function. The size distribution function $F_{V(d)}$ can be frequently approximated by a logarithmic normal distribution (LND), which is uniquely characterized by a median d_{50} and a scatter parameter σ_{ln}. The size distribution function or the spatial distribution density of microbodies can only be determined stereologically based on certain assumptions concerning their shape and orientation. For an average shape with known orientation percentages, the distribution functions of the planes of the sections and chord lengths of the sections for the individual planes can be calculated from the median $d_{50.3}$ and the scatter parameter with allowance for the cardan angle. With the approximation, the optimal values of the distribution function ($d_{50.3}$ and σ_{ln}) can be determined, which provide the best fit of the distribution function of the planes and chord lengths of the sections with the measured histograms of the section planes and chord lengths.

Grain shape of the minerals. The shape of a microbody can be regarded approximately as an ellipsoid with the principle axes a, b and c. With the help of the principal axes of the ellipsoid, the elongation (E = a/b) and flatness (E = b/c) can be derived.

Intergrowth of the minerals. The formation of the boundary surfaces shows how far the individual microbodies are interlocked with each other, i.e. the degree of intergrowth. The intergrowth K_{VW} is defined as the ratio of the "ideal" microbody surface S_I to the "real" surface S_R of the individual phases. The calculation of the "ideal" surface S_I is based on the microbody size distribution with allowance for the microbody shape and the phase volume percentage. The "real" surface S_R is calculated from the three-dimensional rose of intersections.

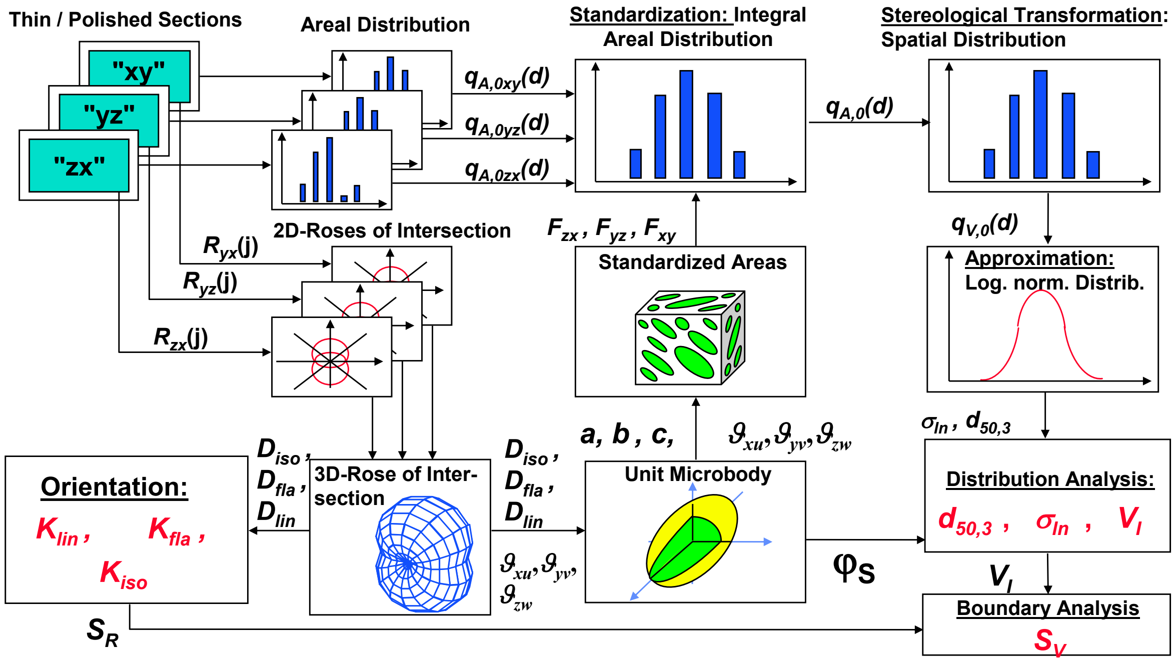

Figure 3 Stereological investigation

Structure

Direction or orientation. The rock fabric is generally not only linear, two-dimensional or non-oriented, but has percentages of linearly and two-dimensionally oriented as well as orientationless boundary surfaces. For characterization, degrees of orientation can be derived from the three-dimensional rose of intersections, which specify the respective boundary surface percentages.

Distribution. Microbodies from one phase can be uniformly distributed in space or also form clusters. In clusters, microbodies of one phase have common boundary surfaces. As a criterion for the evaluation of cluster formation, the definition after Gurland is used (Gurland, 1966), which calculates cluster formation from the ratio of the boundary surfaces between microbodies of the same phase to the total microbody boundary surfaces of this phase.

Relative density. Besides solid phases, a rock also consists of defects which can be filled with gas or liquid. The volume percentage ε_{VH} of these defects can be used for determination of the relative density ε_{VF}.

2. Results of the mathematical-petrographic rock analyses

2.1 Cínovec deposit (Zinnwaldite ores)

The Cínovec-Zinnwald deposit is located in the Erzgebirge region on the border between the Czech Republic and Germany, and is situated in a geologically favorable area known for historic mining of tin, tungsten, and other metals (Figure 4).

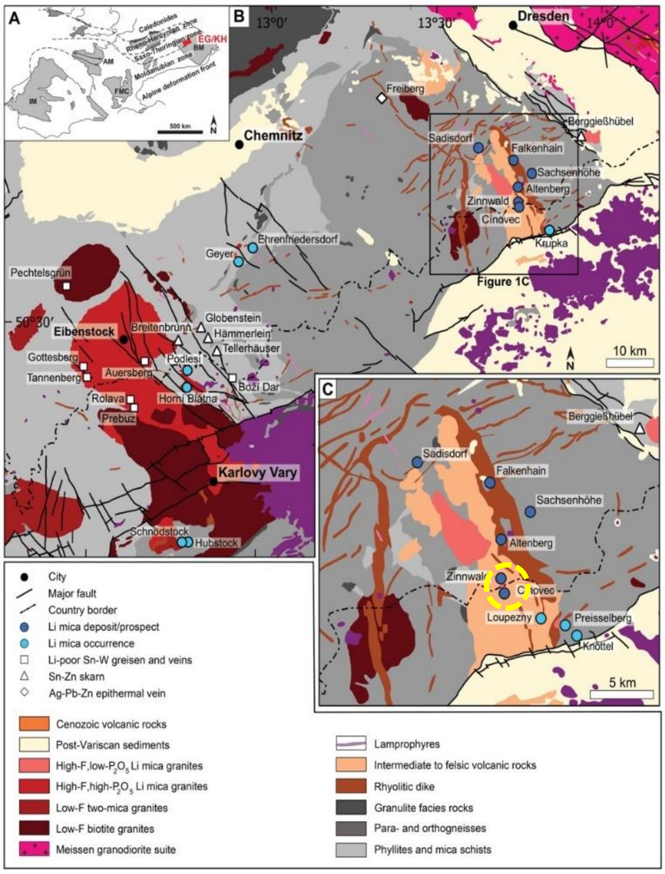

Figure 4 Simplified Variscan basement map (A), regional distribution of greisen-hosted Li mica deposits in the Erzgebirge/Krušné hory (B), and detailed geology of the Altenberg–Teplice caldera (C). Yellow circle is where Cínovec-Zinnwald located (Burisch et al., 2025).

The Cínovec-Zinnwald deposit is hosted within a small, ovoid-shaped albite granite stock that intruded the overlying Teplice Rhyolite and has undergone extensive greisenization, particularly in its apical and marginal zones. This rock is comprising fine to medium-grained albite, quartz, and zinnwaldite, with accessory topaz, fluorite, and alteration minerals such as sericite, illite, and kaolinite (Seifert et al., 2015). Based on recent study by (Burisch, et al., 2025), distinctions exist between the

Zinnwald and Cínovec deposits despite their geological continuity within the same mineralized zone. These differences primarily arise from the more pervasive and voluminous greisen alteration observed at Cínovec, where the alteration forms dome and lens-shaped bodies commonly associated with extensive stockwork veining (Burisch, et al., 2025).

In the summer of 2024, as part of joint efforts, samples were selected for microscopic examination and comminution tests. As a result of preliminary macroscopic analysis, 2 samples were selected for further mathematical-petrographic analysis and physical-mechanical tests: a sample of greisenised granite (GCW-1) and a sample of greisen (GCG-1) (Figure 5). The test results are summarized in Table 1 and Table 2. In terms of optical properties, mica corresponds to zinnwaldite, an intermediate solid-solution series between two end-member siderophyllite-polylithionite minerals. It is possible to determine zinnwaldite in more detail only by electron-microscopic analysis (REM or MLA) or indirectly confirm by chemical analysis.

Figure 5 Greisenised granite (zinnwaldite mica poor GCW-1, left) and greisen (zinnwaldite mica-rich GCG-1, right)

Greisenised granite, GCW-1 (zinnwaldite ore)

The mineralogical composition of GCW-1 was dominated by quartz and feldspar, followed by a smaller proportion of mica, which was interpreted as lithium-bearing mica (zinnwaldite). The volumetric proportion of mica was determined to be approximately 10%. Feldspar occurred in a significantly altered form; in particular, feldspar showed advanced alteration, being partially replaced by clay minerals and carbonates (Figure 6). These alterations were considered to be a contributing factor to the overall reduced strength of the rock. “Non-differentiated” (not analyzed by QMA) phases such as topaz, fluorite, clay minerals, and carbonates were also present in amounts up to 11%.

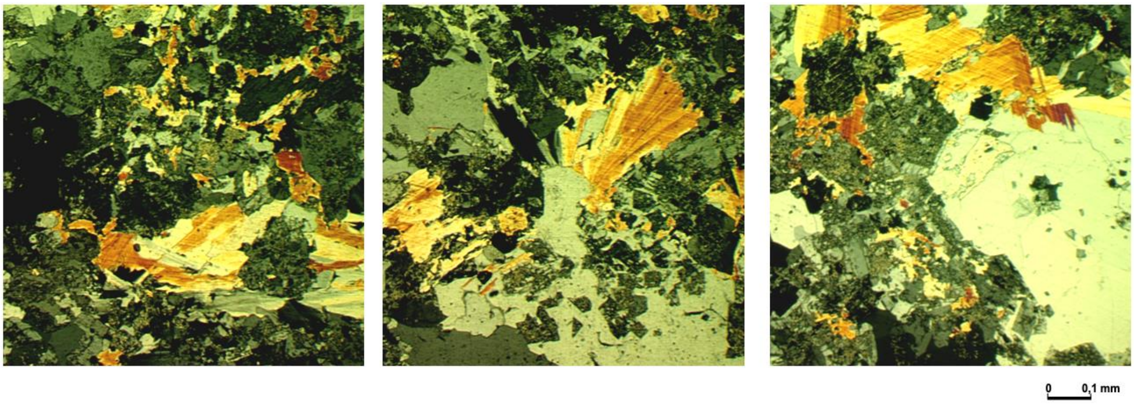

a b c

Figure 6 Selected digitized images of greisenized granite from Cínovec (Czech Republic). 16-x magnified. Thin sections: (GCW-1a,b,c)

In terms of texture, the rock exhibited a disseminated crystalline fabric with a median grain size ($d_{50,3}$) of approximately 3.44 mm (Table 1). The median grain sizes of the main minerals varied notably: quartz grains reached about 2.3 mm, feldspar grains were ca. 4.7 mm, and mica grains approximately 1.3 mm large. The grain size distribution of quartz and mica (zinnwaldite) was relatively moderate, with a logarithmic standard deviation (σ_{ln}) of about 0.5, indicating relatively moderate variation grain dimensions. In contrast, feldspar exhibited a broader size distribution, reflecting significant heterogeneity in grain sizes within these phases.

Raw Material		Kind: Greisenised granite				Phase related features				Raw Materials features
		Deposit: Cinovec	Location: Czech Republic							
Mode		Phases		Art	Kind	Quartz	Fsp	Mica	NDP	Σ Microbodies
		Content	Volumetric Portion	ε_V	%	32	47	10	11	100
Fabric	Texture	Size	Mean diameter	$d_{50,3}$	mm	2,286	4,669	1,322	-	3,437
			Deviation	σ	-	0,578	0,718	0,548	-	0,649
		Articulation	Specific surface	S_V	mm^2/mm^3	6,750	5,27	13,04	-	6,660
		Shape	Elongation	E	-	1,254	1,106	1,236	-	1,174
			Flatness	F	-	1,095	1,33	1,307	-	1,243
		Intergrowth	Degree of intergrowth	K_{VW}	%	63	56	71	-	60
	Structure	Orientation	Degree of linear orientation	K_{lin}	%	16	7	13	-	1
			Degree of areal orientation	K_{fl}	%	5	14	14	-	11
			Degree of isotropic orientation	K_{is}	%	79	79	73	-	88
		Distribution	Degree of clusterisation	C	%	21	21	16	-	21
		Space Filling	Space filling of solid phases	ε_{VF}	%	-	-	-	-	100

NDP - indifferentiated Phases, 11% H=7, Topaz, Calcite, Clay, Fluorite

Table 1: Rock characteristics. Greisenised granite from Cínovec (Czech Republic). Thin sections: 3193,3194,3195 (GCW-1a,b,c)

The shape of the mineral grains, described by their habit and expressed through elongation (E) and flatness (F) ratios. Feldspar grains show a distinct platy habit (E = 1.106, F = 1.330), while mica displays a mixed platy-needle morphology (E = 1.236, F = 1.307), reflecting the layered nature of phyllosilicates. Quartz appears nearly equant and slightly elongated (E = 1.254, F = 1.095). These shape parameters, derived from the ellipsoidal approximation, with elongated and platy grains more likely to fracture along specific structural directions, which may influence breakage patterns during comminution.
A notable result of the stereological analysis was the high degree of mineral roughness within the sample. The overall roughness value (K_R) was approximately 60%, with mica reaching as high as 71%. This indicated a strong interlocking between mica and other mineral phases, particularly quartz and feldspar. This tight bonding makes it harder to separate mica along phase boundaries during crushing or grinding. In addition, the specific surface area (S_V) of the mineral phases was calculated to be around 6.7 mm^2/mm^3. Mica exhibited the highest specific surface among all phases, with a value of approximately 13 mm^2/mm^3, further underscoring its complex geometry and relevance for liberation efficiency. During grinding, once mica is partially liberated, its thin shape causes it to break further (overgrinding) and faster than more compact minerals.
Structurally, the rock structure was predominantly isotropic, with 88% of the mineral boundaries showing random orientation (K_{is}), and only 1% of the mineral boundaries exhibiting linear orientation (K_{lin}). This suggests a non-preferential internal grain arrangement, which could lead to unpredictable fracture behavior under mechanical stress. Furthermore, the clustering degree of quartz and feldspar is relatively low (both 21%), indicating that these grains are generally disseminated and not in direct contact with many grains of the same type. Mica shows the lowest clustering value (16%), meaning it is even more isolated in the rock. This dispersed distribution is beneficial for comminution, as it allows individual grains to break away more easily and may improve mineral liberation.

Greisen, GCG-1 (Zinnwaldite Ore)

GCG-1 sample primarily consisted of quartz and mica (zinnwaldite), with a significantly reduced amount of feldspar compared to the greisenised granite (GCW-1). The zinnwaldite content was determined to be approximately 16% and feldspar reduce to 4%, indicating an increase in mica content as a result of progressive greisenization (Figure 7). Feldspar, in contrast, appeared in minor and less altered forms. Non-differentiate accessory mineral such as topaz, fluorite, carbonates, and clay minerals were present in minor quantities, not exceeding 11% of the total volume. The higher quartz content in GCG-1 contributed to the overall strength and resistance of the rock.

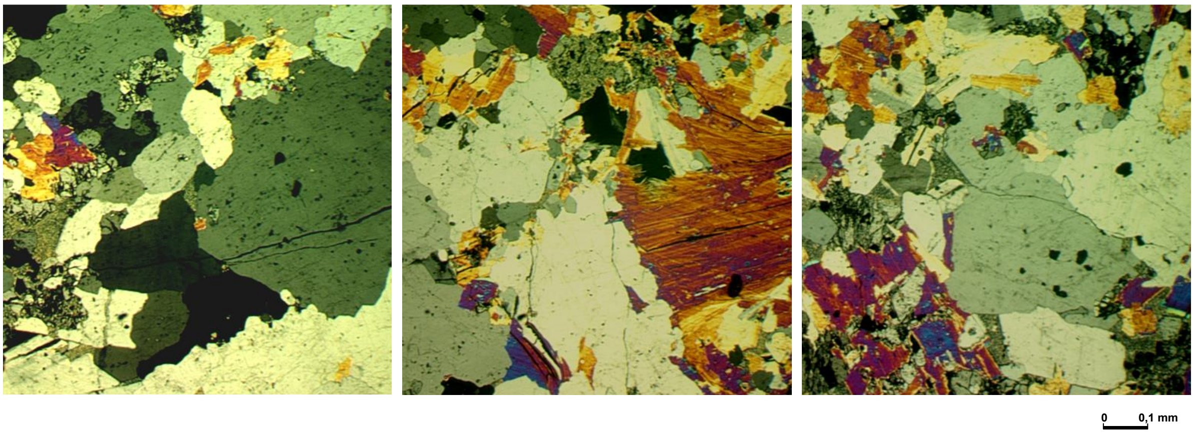

a b c

Figure 7 Selected digitized images of greisen from Cínovec (Czech Republic). 16-x magnified. Thin sections: 3196, 3197, 3198 (GCG-1 a,b,c)

Texturally, GCG-1 exhibited a coarsely crystalline structure with a median grain size ($d_{50.3}$) of approximately 2.23 mm, which was slightly finer than the grain size observed in the greisenised granite (Table 2). Quartz grains maintained porphyroblastic dimensions of around 2.6 mm, while feldspar grains were significantly finer, measuring approximately 1.0 mm. The grain size of zinnwaldite (mica) was approximately 0.7 mm, indicating a significant reduction in grain size compared to GCW-1. Compared to GCW-1, mica in GCG-1 shows a notable reduction in grain size. In terms of grain size distribution, quartz exhibited a relatively broad distribution with a σ_{ln} of 0.640. Mica showed moderate variability σ_{ln} = 0.574, while feldspar, with a σ_{ln} of 0.348, displayed the most uniform grain size among the primary phases. These textural characteristics suggest that GCG-1 underwent more advanced alteration and mineral replacement processes, typical features of progressive greisenization. The finer and more uniform mica in GCG-1 may enhance liberation but could also increase the risk of overgrinding.

The habit of the mineral grains, approximated by ellipsoidal models, reflected the geometric diversity of the constituent phases. Quartz grains in GCG-1 shows slightly elongated form (E = 1.34, F = 1.06), implying strong, compact grains that are more resistant to fracture. Feldspar, due to its limited presence, did not exhibit a dominant geometric trend, while (zinnwaldite), with its distinctly elongated geometry (E = 1.63, F = 1.00), is prone to preferential breakage along its length due to sheet-like crystal structure, potentially leading to thin flakes or fines and overgrinding risk.

The degree of roughness (K_R) between mineral grains was lower in GCG-1 than in the greisenised granite. Overall, the roughness reached approximately 45%, and for mica grains in particular, the value was lower than the 71% recorded in GCW-1. This reduction in interlocking among grains, particularly between mica and quartz, indicated potentially easier liberation of zinnwaldite during mechanical fragmentation. The specific surface area (S_V) of the mineral particles was measured at approximately 6.2 mm^2/mm^3, slightly lower than that of GCW-1. Among all mineral phases, mica again exhibited the highest specific surface area at approximately 11

mm^2/mm^3, which remained an important parameter for its behavior during comminution.

Raw Material		Kind: Greisen					Phase related features				Raw Materials features
		Deposit: Cinovec		Location: Czech Republic							
Mode		Phases			Art	Kind	Quartz	Fsp	Mica	NDP	Σ Microbodies
		Content	Volumetric Portion		ε_V	%	70	4	16	10	100
Fabric	Texture	Size	Mean diameter		$d_{50,3}$	mm	2,646	0,95	0,749	-	2,233
			Deviation		σ	-	0,640	0,348	0,574	-	0,616
		Articulation	Specific surface		S_V	mm^2/mm^3	5,080	8,63	10,75	-	6,250
		Shape	Elongation		E	-	1,340	1,308	1,628	-	1,390
			Flatness		F	-	1,062	1,216	1	-	1,057
		Intergrowth	Degree of intergrowth		K_{VW}	%	45	34	50	-	45
	Structure	Orientation	Degree of linear orientation		K_{lin}	%	20	17	33	-	9
			Degree of areal orientation		K_{fl}	%	3	10	-	-	5
			Degree of isotropic orientation		K_{is}	%	76	72	67	-	86
		Distribution	Degree of clusterisation		C	%	62	13	20	-	52
		Space Filling	Space filling of solid phases		ε_{VF}	%	-	-	-	-	100

NDP - indifferentiated Phases, 10% H=7, Topaz, Calcite, Fluorite

Table 2: Rock characteristics. Greisen from Cínovec (Czech Republic). Thin sections: 3196, 3197, 3198 (GCG-1 a,b,c)

Structurally, GCG-1 displayed predominantly isotropic mineral orientation, similar to GCW-1. Approximately 86% of the mineral boundaries exhibited isotropic orientation (K_{is}), while about 9% showed linear orientation (K_{lin}). The increased proportion of linearly oriented structures compared to GCW-1 (1%) indicated some degree of preferential alignment, although the rock remained largely random in texture.
A significant feature of GCG-1 was the high degree of cluster formation, particularly among quartz grains. Approximately 62% of quartz grains in the sample formed clusters, meaning they shared boundary surfaces with grains of the same mineral phase. This contrasted sharply with GCW-1, where only 21% of quartz grains exhibited clustering. The high clustering coefficient in GCG-1 suggested stronger mutual bonding and interlocking among quartz grains, which contributed to the higher mechanical integrity and higher comminution energy.

2 Villasrubias deposit (Lepidolite ores)

The Villasrubias Lithium Project is an early-stage exploration project located in the southwest corner of the Salamanca province, Castilla y León, Spain, near the Portuguese border and just 33 km from Ciudad Rodrigo. It lies within Central Iberian Zone (CIZ) of the Iberian Massif, one of the most geologically significant regions for lithium exploration in Europe, hosting several other lithium and tin-bearing deposits in Spain and Portugal (Figure 8). This project is associated with lepidolite-subtype granitic pegmatites of the LCT (lithium–cesium–tantalum) family. These pegmatites are genetically linked to the highly evolved, S-type Cadalso–Casillas de Flores granitic batholith and were emplaced into metamorphic rocks of the Schist–Greywacke Complex (CEG) (Llorens and Moro, 2010). Preliminary exploration conducted by SIEMCALSA, a government-backed entity in Castilla y León between 2017 and 2020, identified lithium-bearing minerals including lepidolite and lithium-muscovite, as well as cassiterite, tantalum, and niobium, with petrographic and geochemical analyses returning Li_2CO_3 grades of up to 0.88% and an average of 0.52% in lepidolite-rich apo-pegmatites (Guijarro, 2022, Table 1). The pegmatite group is also known under name “La Canalita pegmatites” (Llorens and Moro, 2010).

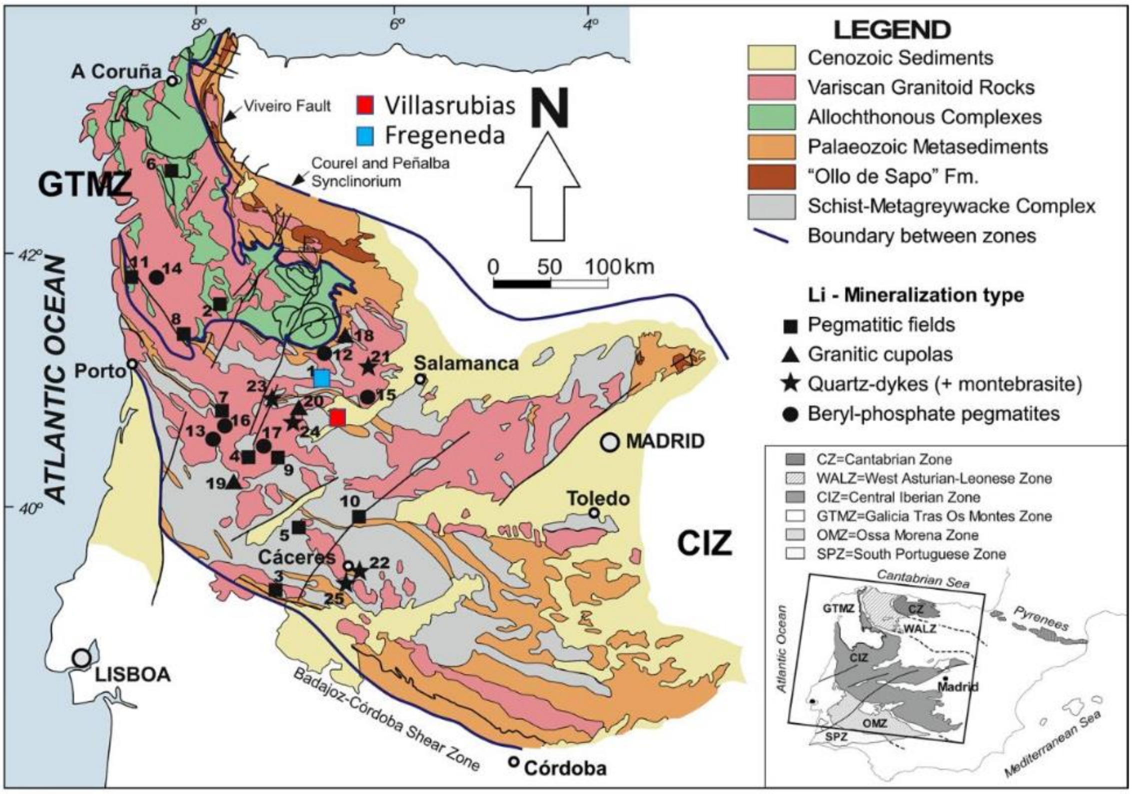

Figure 8 Schematic geological map of the Central Iberian Zone (CIZ) and the Galicia-Trás-Os Montes Zone (GTMZ) (Spain and Portugal) with the location of the different Li-mineralization and the Villasrubias project (Roda-Robles et al., 2016)

As a result of preliminary macroscopic analysis, 2 samples were selected for further mathematical-petrographic analysis and physical-mechanical tests: a sample of lepidolite-bearing aplite containing a few amount of lepidolite (LSA-1) and a sample of layered feldspar-lepidolite pegmatite as a sample of rich lepidolite ore (LSR-1) (Figure 5 Greisenised granite (zinnwaldite mica poor GCW-1, left) and greisen (zinnwaldite mica-rich GCG-1, right)

The test results are summarized in Table 3, Table 4.

Figure 9 lepidolite-bearing aplite (LSA-1), left) and feldspar-lepidolite pegmatite (LSR-1, right)

Lepidolite belongs to the Trilithionite- Polylithionite Series which ideally contains between 2.61 and 3.00 wt. % of lithium. The pink-purple colour characteristic of lithium-muscovite and lepidolite is usually attributed to manganese or iron in the mica structure. In any case, further mineralogical studies are required to clarify the detailed mineral composition. Hereinafter mica will be conventionally referred to as "lepidolite".

Lepidolite-bearing aplite, LSA-1 (Lepidolite Ore)

The LSA-1 sample, interpreted as a lepidolite-bearing aplite, is composed primarily of quartz (45%), feldspar (31%), and mica (20%), with a minor portion (4%) consisting of non-differentiated phases such as topaz and fluorite (Figure 10). The phase distribution reflects a moderately heterogeneous mineralogical fabric, with quartz as the dominant component and feldspar and mica in subordinate but significant proportions.

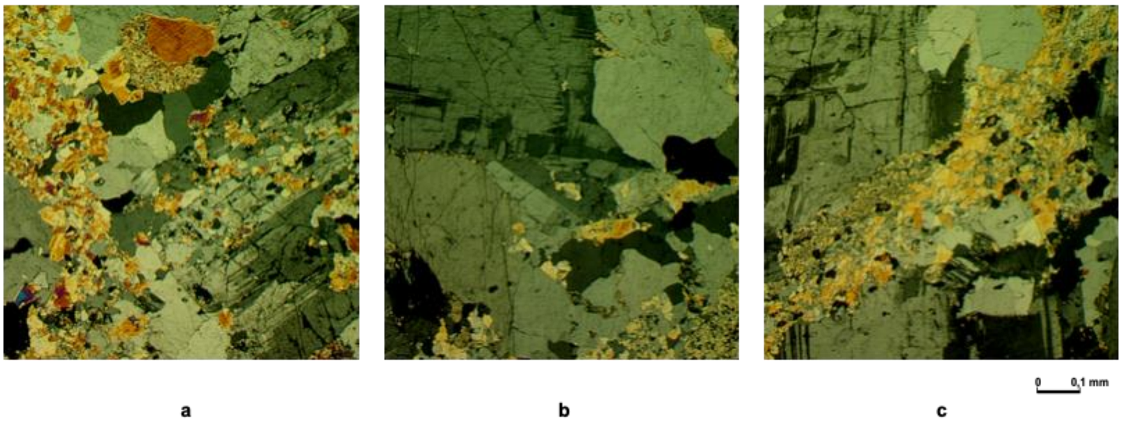

Figure 10 Selected digitized optical microscopy images of lepidolite-bearing aplite from the Villasrubias deposit (Spain). Crossed polars, 16-x magnified. Thin sections (LSA-1a,b,c).

Texturally, LSA-1 exhibits a fine-grained structure, with an overall median particle diameter ($d_{50\text{-}3}$) of 0.318 mm (Table 3). Among the major phases, feldspar has the largest grain size (0.495 mm), followed by quartz (0.289 mm), while mica (lepidolite) is the finest-grained phase, averaging only 0.103 mm. This large grain size contrast suggests that mica occurs as fine inclusions or small interstitial flakes within the coarser quartz and feldspar matrix. The particle size distribution, expressed by standard deviation (σ), also highlights textural variability. Mica has the narrowest distribution (σ = 0.302), indicating a relatively uniform grain size. Quartz shows a broader spread (σ = 0.408), and feldspar displays the widest distribution (σ = 0.454), reflecting the greatest internal heterogeneity among the three phases.

Raw Material		Kind: lepidolite-bearing aplite				Phase related features				Raw Materials features
		Deposit: Villasrubias	Location: Spanien							
Mode		Phases		Art	Kind	Quartz	Fsp	Mica	NDP	Σ Microbodies
		Content	Volumetric Portion	ε_V	%	45	31	20	-	100
Fabric	Texture	Size	Mean diameter	$d_{50,3}$	mm	0,289	0,495	0,103	-	0,318
			Deviation	σ	-	0,41	0,454	0,302	-	0,401
		Articulation	Specific surface	S_V	mm^2/mm^3	19,95	9,02	27,29	-	17,91
		Shape	Elongation	E	-	4,00	2,42	1,51	-	2,98
			Flatness	F	-	1,68	1,24	1,05	-	1,41
		Intergrowth	Degree of intergrowth	K_{VW}	%	44	24	10	-	30
	Structure	Orientation	Degree of linear orientation	K_{lin}	%	50	46	28	-	52
			Degree of areal orientation	K_{fl}	%	29	12	3	-	18
			Degree of isotropic orientation	K_{is}	%	21	42	69	-	31
		Distribution	Degree of clusterisation	C	%	45	20	18	-	31
		Space Filling	Space filling of solid phases	ε_{VF}	%	-	-	-	-	100

NDP - indifferentiated Phases, 4% H=6, Topaz, Fluorite

Table 3: Rock characteristics. Lepidolite granite-greisen from Villasrubias (Spanien). Thin sections: 3201,3202,3203 (LSA-1a,b,c)

Grain shape analysis of the LSA-1 indicate that quartz shows needle-like structure (E = 4.008, F = 1.675) and Feldspar also displays an elongated habit (E = 2.415, F = 1.238), though to a lesser extent. The needle-like and platy habit of quartz observed in LSA-1 is quite unusual for quartz, this morphology likely developed through post-magmatic processes such as hydrothermal alteration, platy habit of quartz needs to be checked using REM. Mica shows a more needle-shape, slightly equant geometry, with an elongation of 1.514 and flatness of 1.052. The overall elongation value of 2.975 for the bulk sample indicates a general tendency toward elongated grain shapes.
The specific surface area (S_V) of the particles varied significantly across the phases. Mica (lepidolite) exhibited the highest specific surface area at 27.29 mm^2/mm^3, followed by quartz (19.95 mm^2/mm^3) and feldspar (9.02 mm^2/mm^3). The overall specific surface area of the rock was estimated at 17.91 mm^2/mm^3. The high surface area of mica underscored its high liberation potential but also an increased risk of overgrinding during comminution. The degree of roughness (K_R) reflected how tightly mineral phases were bonded. Quartz showed a relatively high degree of roughness at 44%, feldspar at 24%, and mica (lepidolite) at 10%, resulting in an average degree of roughness of 30%. The low degree roughness of mica suggests it

is weakly bonded to adjacent minerals, making it more favorable for mechanical separation with less energy input.

Structurally, the LSA-1 sample exhibits a quite moderate anisotropic orientation with total degree of isotropic orientation 31%, with strong linear orientation in quartz (K_{lin} = 50%) and feldspar (46%). Mica shows a lower linear alignment (28%) and high isotropy (K_{is} = 69%), indicating a more random distribution. The areal orientation (K_{fl}) is moderate in quartz 29% but low in feldspar 12% and mica (3%), confirming that mica grains are not directionally aligned. These patterns suggest that fracture propagation may be partially guided by mineral alignment in quartz and feldspar, whereas mica likely fractures independently of fabric orientation.

Clustering analysis reveals that quartz has the highest aggregation tendency (C = 45%), forming phase-bound domains that may resist early disintegration. Feldspar and mica show lower clustering values (20% and 18%, respectively), with mica being the most spatially dispersed. This dispersed distribution supports easier mechanical liberation of mica and means it is less locked in with other minerals, although it may also make it more vulnerable to overgrinding.

Lepidolite-feldspar pegmatite, LSR-1 (Lepidolite Ore)

The modal composition of the sample and its mineralogical composition is consistent with layered lepidolite-feldspar pegmatite. Modal analysis reveals a dominance of quartz (38 vol%) and lithium-rich mica, likely lepidolite (34 vol%), accompanied by subordinate feldspar (15 vol%) and accessory phases such as topaz and fluorite within the undifferentiated mineral portion (13 vol%). The textural analysis shows a fine- to medium-grained structure, with median grain sizes of 0.257 mm for quartz, 0.272 mm for feldspar, and 0.223 mm for mica, indicating a non-pegmatitic character. The reduced feldspar content and enrichment in lithium mica and accessory minerals reflect intense hydrothermal alteration (Figure 11).

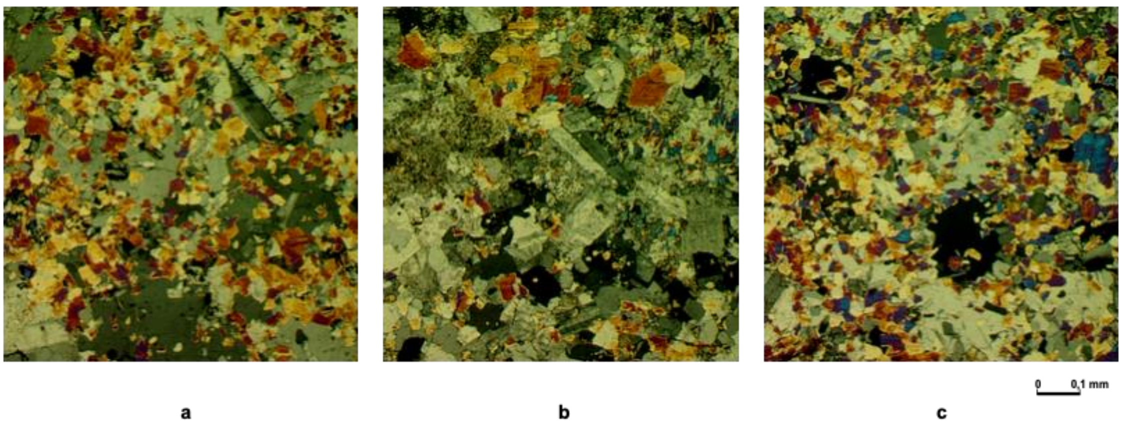

Figure 11 Selected digitised optical microscopy images of lepidolite-feldspar pegmatite from the Villasrubias (Spain). Crossed Polars. 16-x magnified. Thin sections (LSR-1a,b,c).

The overall average grain shape (E = 1.297, F = 1.105) reflects a near-equant grain distribution with no extreme geometries. Mica (lepidolite) shows the highest elongation (E = 1.35) but a flatness of 1.00, suggesting a slightly elongated but compact form. Quartz and feldspar are similarly shaped, with elongation values of 1.284 and 1.209, and flatness values of 1.185 and 1.140, respectively. These moderate shape parameters imply that particle breakage during comminution is expected to be relatively uniform, though mica remains more susceptible to early fragmentation due to its structural cleavage.

The specific surface area (S_V) of LSR-1 varies notably among mineral phases. Mica (lepidolite) displays the highest SV at 24.63 mm^2/mm^3, followed by quartz (18.73 mm^2/mm^3) and feldspar (16.49 mm^2/mm^3). The overall SV of the sample is 20.68 mm^2/mm^3, indicating a high degree of surface development. The elevated SV of mica reflects its fine, platy morphology and suggests a high potential for liberation during grinding but also highlights its susceptibility to overgrinding due to increased exposure and structural weakness. The degree of roughness (K_R) further supports these observations. Quartz shows the highest interlocking at 31%, while feldspar and mica exhibit lower roughness values of 16% and 14%, respectively. The overall roughness degree is 22%, indicating moderate interparticle bonding. The relatively low roughness of mica suggests it is weakly interlocked in the matrix, offering favorable conditions for its selective liberation during mechanical fragmentation.

The clustering coefficient (C) in LSR-1 indicates that quartz grains have the highest tendency to form aggregates (26%), followed by mica (23%) and feldspar (17%), with an overall clustering degree of 24%. These values reflect a moderate level of mineral clustering, where individual phases are partially associated but not extensively interlocked. Structurally, the rock shows a highly isotropic orientation structure (K_{is} = 80%), with low values for linear and areal orientation across all phases. This combination of moderate clustering and isotropic alignment suggests a texture favorable for disintegration during comminution, where grains are more likely to separate independently rather than breaking through strongly bonded aggregates.

QMA confirms that all samples represent quartz-dominant granitoid lithologies, with variable mica contents. The Cínovec samples (GCW-1 and GCG-1) show a coarser-grained texture of mica (0.75 – 1.3 mm) compared to the Villasrubias samples (LSA-1 and LSR-1), which are significantly finer grained (~0.25 mm).

Raw Material		Kind: feldspar-lepidolite pegmatite				Phase related features				Raw Materials features
		Deposit: Villasrubias	Location: Spanien							
Mode		Phases		Art	Kind	Quartz	Fsp	Mica	NDP	Σ Microbodies
		Content	Volumetric Portion	ε_V	%	38	15	34	13	100
Fabric	Texture	Size	Mean diameter	$d_{50,3}$	mm	0,257	0,274	0,223	-	0,246
			Deviation	σ	-	0,378	0,334	0,356	-	0,362
		Articulation	Specific surface	S_V	mm^2/mm^3	18,730	16,49	24,63	-	20,680
		Shape	Elongation	E	-	1,284	1,209	1,35	-	1,297
			Flatness	F	-	1,185	1,14	1	-	1,105
		Intergrowth	Degree of intergrowth	K_{VW}	%	31	16	14	-	22
	Structure	Orientation	Degree of linear orientation	K_{lin}	%	17	13	22	-	14
			Degree of areal orientation	K_{fl}	%	9	7	-	-	5
			Degree of isotropic orientation	K_{is}	%	75	80	78	-	80
		Distribution	Degree of clusterisation	C	%	27	17	23	-	24
		Space Filling	Space filling of solid phases	ε_{VF}	%	-	-	-	-	100

NDP - indifferentiated Phases, 14% H=6, Topaz, Fluorite

Table 4: Rock characteristics. Lepidolite greisen from Villasrubias deposit. Thin section (LSR-1a,b,c)

The degree of roughness (K_R) of mica was higher in GCW-1 (71%) than in GCG-1 (50%), this tightly intergrown textures of GCW and GCG require higher breakage energy, careful control of grinding conditions, and may limit early-stage liberation. In contrast, lepidolite in the Villasrubias samples exhibits a much lower roughness (10–14%), suggesting weaker bonding to adjacent phases and easier detachment during mechanical comminution.

Although lepidolite-bearing ores show lower interlocking/degree of roughness, their finer grain size may also present higher comminution resistance. This is attributed to their compact and cohesive mineral textures, which enhance the mechanical integrity of the rock and hinder effective liberation of lithium mica during grinding. Structurally, both zinnwaldite and lepidolite samples exhibit a high degree of isotropy (K_{is} = 80–88), except in samples in lepidolite low mica content. This predominantly random internal grain orientation supports more uniform stress distribution during breakage, potentially leading to more predictable fracture behavior under mechanical loading.

2.3 Presqueira pegmatite (Petalite ores)

Presqueira petalite deposit lies near the village Cerdedo (Pontevedra, Galicia, Spain), about 75 km from Ourense and 35 km from Cháves in NW Spain. Geologically, it is located within Central Iberian Zone of the Iberian Massif and associates with granitic-pegmatites rocks (black square nr. 6 on Figure 8, Lleira et al. 2019). The grain size of rocks is moderately heterogeneous, with aplitic and pegmatitic facies sometimes with large crystals (4-6 cm long). Layering is relatively common in the granitic rocks/pegmatites (Figure 12, left, center). The main minerals present macroscopically

are quartz, feldspar, light mica, petalite and iron oxides/hydroxides. The main Li-bearing mineral is petalite, partly substituted to a quartz-spodumene mass (Figure 13, a, b) and are accompanied with optically isotropic pollucite or garnet (Figure 13, c). Macroscopic petalite typically occurs in white subhedral to almost euhedral crystals that rest within albitic units of the pegmatites (Dittrich et al., 2020).
According to preliminary investigations three groups were classified (Figure 12). At present only preliminary petrographic analysis has been carried out. QMA analysis will be provided in the final report.

Figure 12 petalite granitic rock (PSF-1, left), weathered petalite granitic rock (sample PSW-2, centre) and petalite granite pegmatite (PSQ-3, right)

Petalite granitic rock (PSF-1)

The first group shows white in colour, slightly yellowish, predominantly consist of quartz with feldspars (albite, K-Feldspar), white mica (Muscovite or/and lepidolite), with light layering. Mica displays a slightly preferred orientation, which could be indicative of a foliated or layered structure. Petalite and spodumene are present in small quantities. Amount of petalite does not exceed 5%, grains are distributed evenly throughout the rock mass. Spodumene-quartz mass replaces petalite in thin veins up to 0.2 mm thick and in very fine-grained aggregates rimming the petalite grains (Fig. 13a, b). The general texture of the rock is medium-grained, there is a slight schistosity due to the location of mica crystals and feldspars (Figure 13).

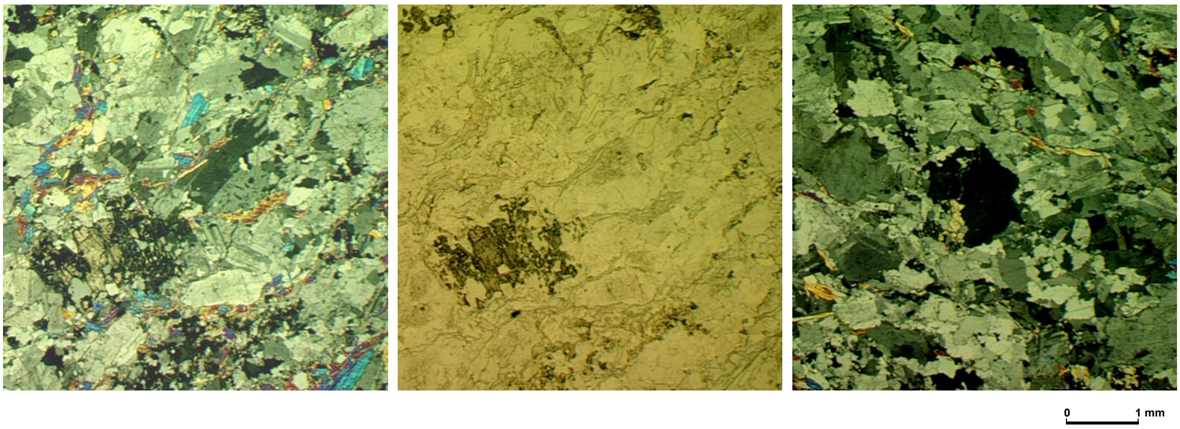

a b c

Figure 13 Selected digitized images of Petalite granitic rock (PSF-1 from Salamanca deposit (Spain). 16-x magnified. Thin sections: PSF-1a,b,c, b – ppl

«Weathered» petalite granitic rock (PSW-2)

The rock appears predominantly white with brownish colour, likely resulting from surface weathering and iron-oxide staining. The mineral assemblage includes quartz, feldspar mica, and petalite with spodumene.

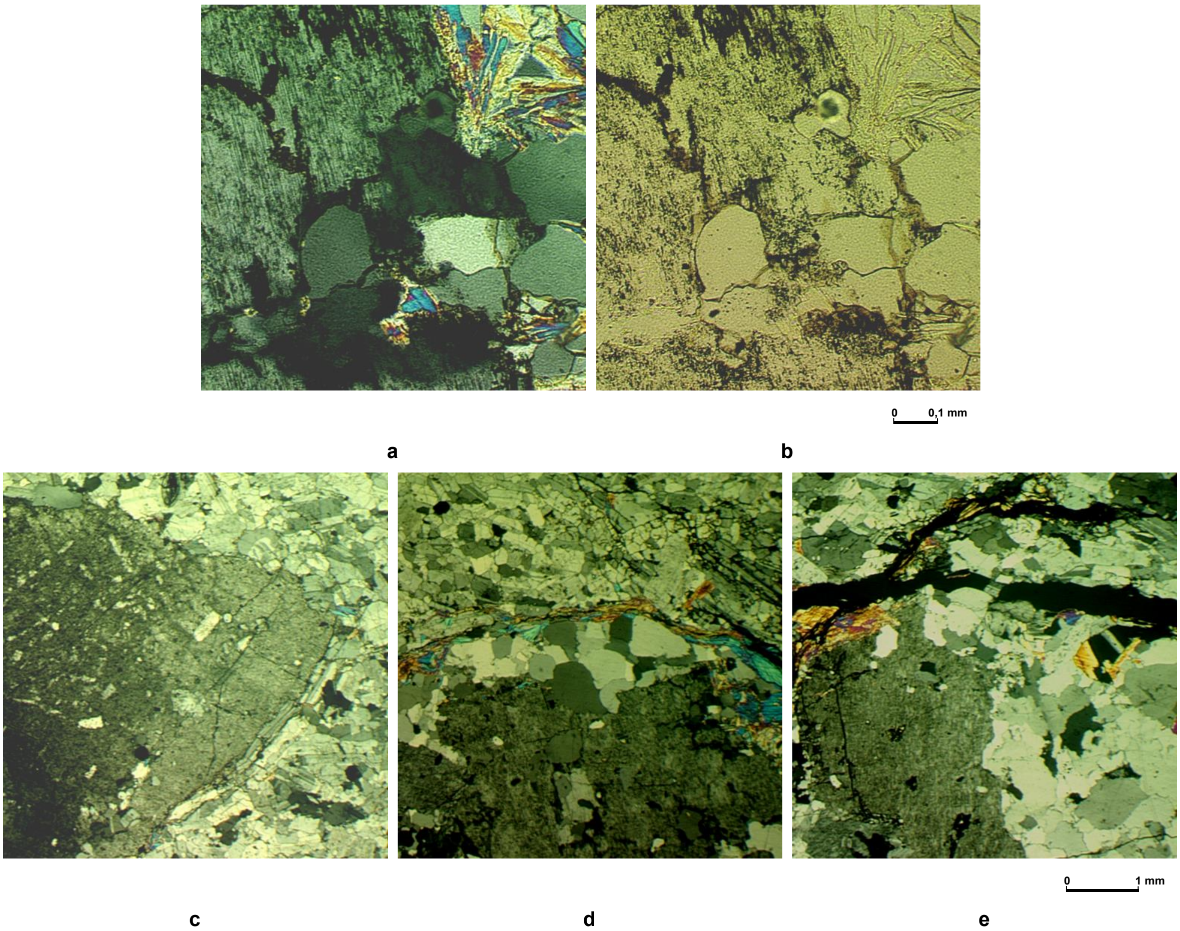

Figure 14 Selected digitized images of Weathered petalite granitic rock (PSW-2) from Salamanca deposit (Spain). a, b - 100-x magnified, c-e – 16-x magnified. Thin sections: PSW-2a,b,c. b - ppl

Although very similar to the surrounding albite, petalite can be easily distinguished by its prominent (001) cleavage plane (Figure 14). Petalite is further characterised by tiny inclusions of mica, feldspar (albite) and quartz. Grain sizes are very heterogeneous. Petalite crystals are rare (5-8% of the mass) and reach 4-5 mm against the background of the remaining fine-crystalline mass of quartz-feldspar-mica (with an average size of 0.3-0.6 mm).

Petalite granite pegmatite (PSQ-3)

This unit has a greyish colour and is dominated by petalite, quartz, white mica, feldspar. Almost the entire surface of the thin-section is represented by large petalite crystals (2-6 cm long) with "inclusions" of tabular feldspar crystals (up to 0.2 mm in size), as well as veins of quartz-spodumene or mica.

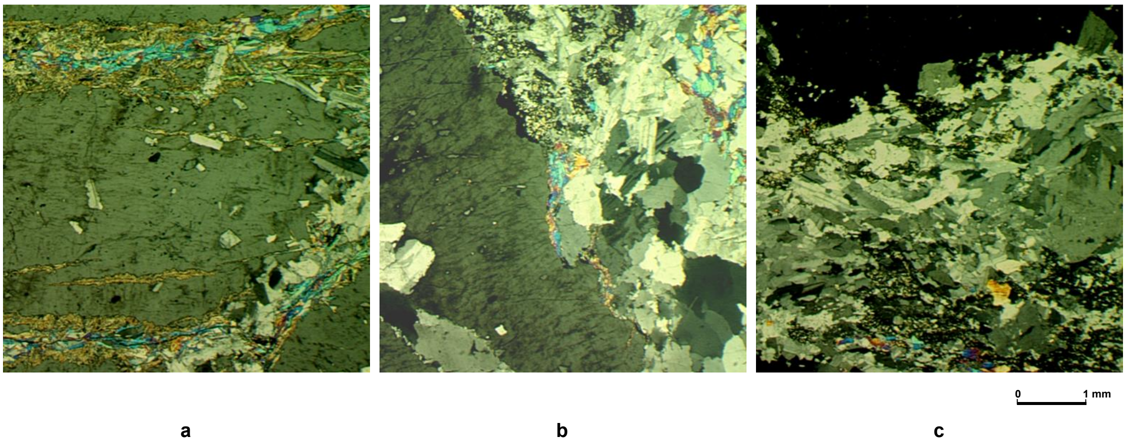

Figure 15 Selected digitized images of petalite granite pegmatite (PSQ-3) from Salamanca deposit (Spain). 16-x magnified. Thin sections PSQ-3a,b,c.

The layering of the rock is clearly evident, expressed in the distribution of feldspar and mica crystals. Quartz often has an uneven surface of grains, which also indicates specific conditions of rock transformation. Based on the grain size, the rock can be classified as a petalite pegmatite. The petalite content in the rock reaches 60-70%, which, given the size, of course, makes it difficult to quantify the petalite content in the entire group. For a more detailed analysis, all three groups of rocks were sent for chemical analysis, the results of which will also be provided in the final report.

3. Chemical Analyses

The lithium content in the studied samples was determined by ICP-OES (inductively coupled plasma optical emission spectroscopy) at the Institut für Technische Chemie, TUBAF. The results of lithium content in petalite ores are not ready yet and will be provided with a final report.

The reference sample (lepidolite-ref OREAS 750b) was used in the analysis. As can be seen from the Table 5, the division of rocks by mica content is obviously comparable with the lithium content. Thus, the minimum lithium content characterizes zinnwaldite-poor ores (1518 ppm), and the maximum lithium content in lepidolite-rich ores (4462.8 ppm).

Ore type	**Li, ppm**
Zinnwaldite-poor (Greisenised granite, GCW-1)	1518.0
Zinnwaldite-rich (Greisen, GCG-1)	4301.1
Zinnwaldite-mix	2395.4
Lepidolite-rich (feldspar-lepidolite pegmatite, LSR-1)	4462.8
Li-poor (Lepidolite-bearing aplite, LSA-1)	3409.2
Lepidolite-Ref	2265.8

Table 5: Lithium content in the studied rocks according to ICP-AS results

4. Determination of Vickers Microhardness and Fracture Toughness in studied rocks

The Vickers microhardness test is a method used to measure the hardness of materials on a microscopic scale, especially useful for small, thin, or surface-treated specimens. This test uses a diamond-shaped indenter with a four-sided pyramidal geometry to create a small indentation on the material's surface.
The Vickers microhardness test uses a diamond indenter with a four-sided pyramidal geometry (square base with an angle of 136° between opposite faces). It is pressed into the material's surface under a small load, typically ranging from a few grams to 1 kgf (kilogram-force), to create a microscopic indent (Kuangdi, 2024). The Vickers Hardness Number (HV) is calculated in Eq. **¡Error! No se encuentra el origen de la referencia.**:

$$HV = \frac{1.854 \cdot F}{d^2} \tag{1}$$

Where
F is the applied load in kgf,
d is the average diagonal length in millimeters.
Another important parameter obtained from the Vickers microhardness test is fracture toughness (Kic). It is defined as the critical value of the stress intensity factor at which a crack starts to grow rapidly and uncontrollably. This property is especially relevant for brittle materials and reflects their resistance to crack propagation under tensile loading. As load is applied to a material with an existing crack, the stress at the crack tip increases. Once this stress reaches a critical threshold the crack extends suddenly, leading to failure (Quinn & Bradt, 2007).
When the applied force exceeds this first critical limit, the internal stresses become high enough to form small surface cracks at the corners of the indentation upon unloading. These are known as Palmqvist cracks and extend outward along the diagonals of the indentation (Figure 16) (Moradkhani et al., 2023). These cracks form under relatively low indentation loads and are measured from the edge of the indent to the crack tip. This model is typically observed in tougher or less brittle materials, where the cracks remain near the surface and do not penetrate deeply.

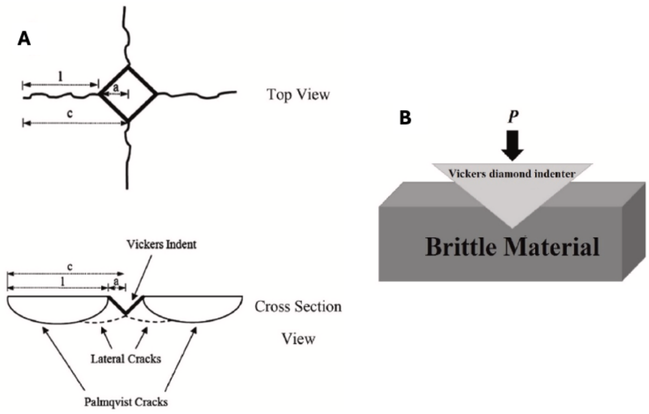

Figure 16: Schematic of a) Palmqvist crack model, and c) Vickers diamond indenter in brittle material (Moradkhani et al., 2023)

Based on Schriber's work, fracture toughness can be determined empirically through indentation fracture mechanics, which provides a practical alternative to conventional large-scale fracture tests. This method is particularly suitable for dense, brittle materials and fine-grained mineral structures where sample preparation for standard tests may be limited. The approach is based on principles from linear elastic fracture mechanics (LEFM), in which the stress intensity at the tip of a crack is a critical factor in predicting crack propagation. The relationship between the applied load and the resulting crack geometry forms the basis for estimating fracture toughness (Schreiber, 2018).

$$\boldsymbol{K_{ic}} = \frac{\boldsymbol{F}}{(\pi \cdot \boldsymbol{c})^{\frac{3}{2}} \cdot \boldsymbol{tan}\, \alpha} \qquad (2)$$

Where

F is applied load (N)

c is is the crack length measured from the center of the indentation to the crack tip (in meters),

α is the half-angle of the Vickers pyramid, equal to 68°.

This simplified formulation **¡Error! No se encuentra el origen de la referencia.** omits the need for direct measurement of Young's modulus (E) and hardness (H) which are typically required in more formal models such as that of (Anstis et al., 1981). Instead, the geometry of the indenter and the crack length are used directly, making the method accessible and efficient for comparative studies.

In the context of this study, Vicker Microhardness and fracture toughness tests are applied to the main identified minerals in the lithium-mica ore. These measurements provide insights into the mechanical response of each mineral phase, offering a deeper understanding of their breakage behaviour under applied stress. This information is essential for evaluating mineral liberation potential and optimizing comminution strategies.

The test was performed using a Shimadzu HMV-G21DT Micro Vickers Hardness Tester (Figure 17), equipped with a diamond Vickers pyramid indenter (a four-sided pyramid with a dihedral angle of 136°). The instrument includes an integrated optical system, along with a specimen base to secure the prepared sample.

Figure 17: a) Polished section from Cínovec and Villasrubias b) specific mineral for microhardness characterisation c) microhardness device

The specimen surface was required to be flat, polished, and free from surface irregularities. A controlled load, typically ranging from 0.098 to 1.961 N depending on the mineral tested, was applied to the indenter and held for 15 seconds. After unloading, the indentation was examined and measured under the microscope. In addition, crack patterns surrounding the indentation, crack lengths (c) were measured using the optical system to determine the fracture toughness, particularly for brittle materials (Figure 18). To ensure statistical reliability, 15 to 20 measurements were collected for each mineral.

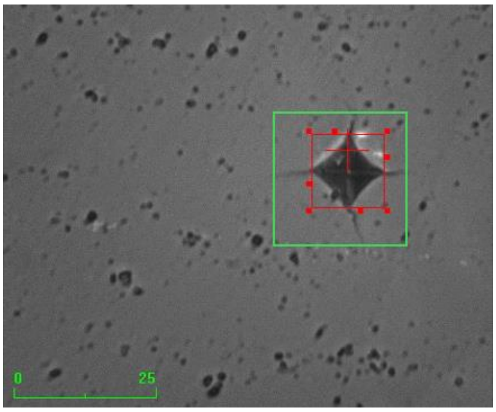

Figure 18: Indentation crack pattern from the Micro Vickers Hardness Test. The red square indicates the indentation diagonal used for hardness measurement, while the green square marks the crack length used to estimate fracture toughness

Kind	Mineral	Content (%)	Grain size (mm)	Vickers hardness number (HV)	Specific surface (mm^2/mm^3)	Fracture toughness ($MN/m^{3/2}$)
Greisenised granite (Zinnwaldite Poor - GCW)	Quartz	32	2,286	1234.36 ± 94.72	6,7	2.11 ± 0.5
	Feldspar	47	4,669	903.0 ± 111.85	5,27	1.48 ± 0.51
	Mica	10	1,322	154.51 ± 48.63	13,04	0.52 ± 0.10
Greisen (Zinnwaldite Rich - GCG)	Quartz	70	2,286	1290.9 ± 66.87	5,08	2.39 ± 0.34
	Feldspar	4	4,669	740.369 ± 118.4	8,63	1.47 ± 0.63
	Mica	16	1,322	194.9 ± 49.06	10,75	0.61 ± 0.10
Lepidolite-bearing aplite (Lepidolite Poor - LSA)	Quartz	45	0,289	1149.73 ± 103.2	19,95	2.24 ± 0.59
	Feldspar	31	0,495	838.72 ± 84.96	9,02	1.55 ± 0.42
	Mica	20	0,103	167.11 ± 40.36	27,29	0.59 ± 0.14
Lepidolite-feldspar pegmatite (Lepidolite Rich - LSR)	Quartz	38	0,257	1302.70 ± 132.92	18,73	2.49 ± 0.66
	Feldspar	15	0,274	879.17 ± 105.60	16,49	2.06 ± 0.75
	Mica	34	0,223	179.05 ± 42.70	24,63	0.66 ± 0.21
Pegmatite (Petalite)	Petalite	-	-	908.00 ± 155.11	-	1.49 ± 0.55

Table 6: Vickers Microhardness test of the studied rocks

From the Vickers microhardness test, mica consistently shows the lowest hardness (154–195 N/mm²), compared to quartz and feldspar, which present significantly higher values. Quartz shows the highest Vickers hardness (1234–1302 N/mm²) and fracture toughness (2.11–2.49 $MN{\cdot}m^{-3/2}$), indicating strong resistance to deformation and crack propagation. Feldspar, while slightly softer (740–903 N/mm²) and less tough (1.47–2.06 $MN{\cdot}m^{-3/2}$), remains high relative to mica. (Table 6). Petalite shows a similar picture with average Vickers microhardness 611–1199 N/mm² and fracture toughness (0.78–3.2 $MN{\cdot}m^{-3/2}$), which corresponds with reference data (Hunger et al., 2010; Luo et al., 2022).

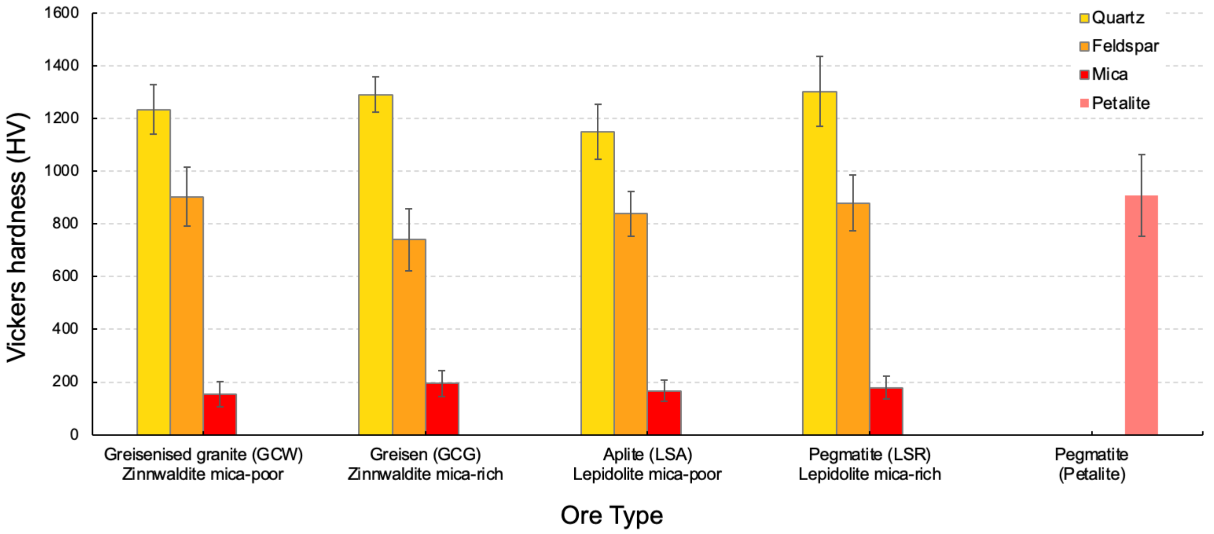

Figure 19: Vicker hardness of mineral across different type lithium ores.

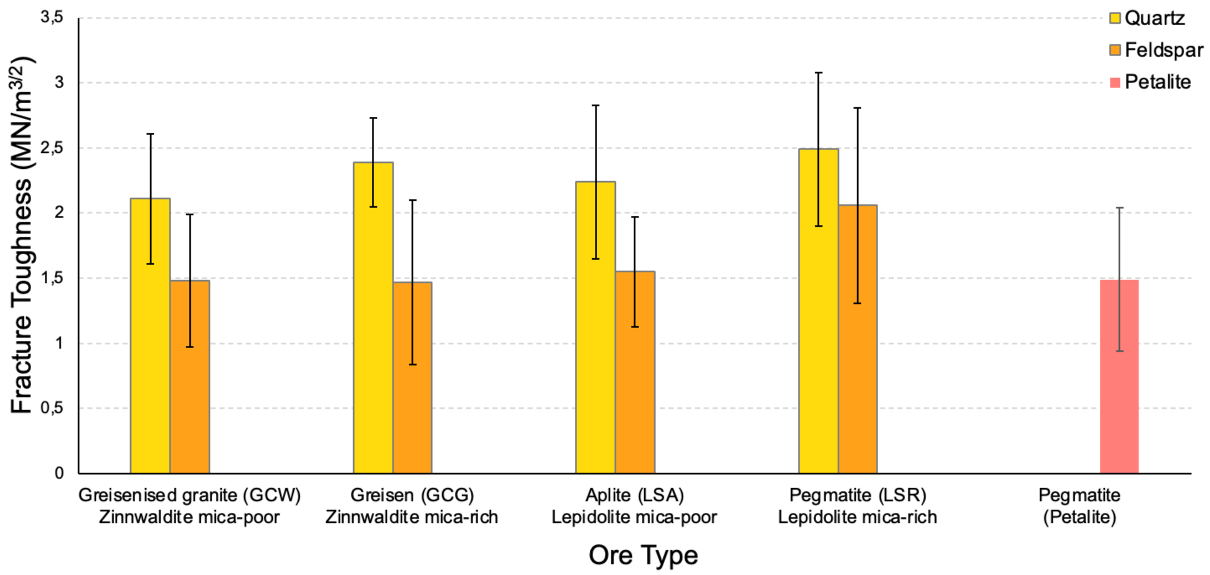

Figure 20: Fracture toughness of mineral across different type lithium ores.

Mica is a soft and flexible mineral with perfect cleavage, meaning it easily splits along certain planes. Because of its crystal structure, mica can deform plastically, changing shape without forming cracks (see Figure 21a). During testing, it was not possible to apply enough force to create measurable cracks without completely breaking the grain. As a result, its fracture toughness could not be determined.

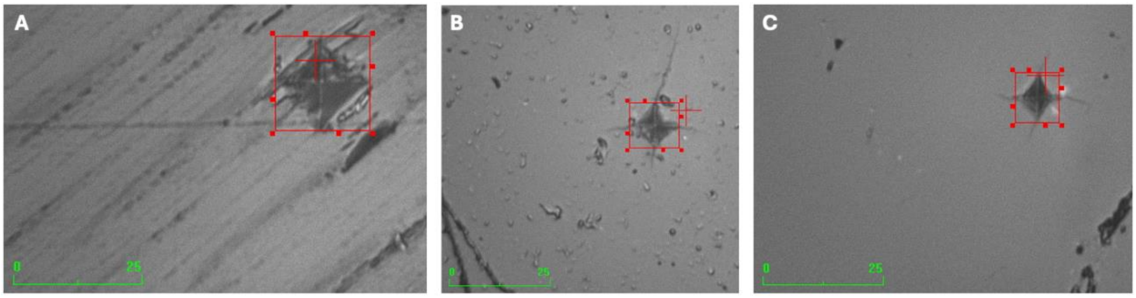

Figure 21: Vickers Hardness microindentation investigation. a) Mica mineral showed perfect cleavage. b) Primary radial crack on quartz. c) Primary radial crack on feldspar.

These findings indicate that both lithium-bearing ores show a pronounced mechanical contrast between the lithium micas and their associated gangue minerals. A similar observation was made by (Hesse, 2017), noted that minerals with significantly lower hardness are often indicative of favorable conditions for selective mineral liberation. In the case of zinnwaldite, its relatively high grain boundary roughness based on QMA, suggests that breakage is more likely to occur preferentially within the mineral rather than along the interfaces. Conversely, for lepidolite, the relatively low roughness contrast between lepidolite and its surrounding gangue minerals, as identified through QMA, may facilitate interfacial breakage and thus promote more efficient mineral liberation.
This noticeable difference establishes mica as the mechanically weakest phase in the mineralogical assemblage, making it highly susceptible to preferential fragmentation under moderate energy input. Such characteristics are advantageous for selective comminution strategies, where energy can be optimized to preferentially fracture the softer lithium-bearing phases while minimizing breakage of the harder gangue components.

4. Determination of Point Load Strength Index of Rocks

The Point Load Test (PLT) is a simple, quick, and practical field method used to estimate the strength of rock materials. PLT is useful when there are limited core sample or when uniaxial compression tests (UCS) are not feasible due to time, cost, or equipment constraints. It involves applying a concentrated load to a rock sample, either a cylindrical core, a disc, or an irregular lump (Figure 22), using two conical platens until the rocks fails. The primary purpose of the test is to determine the Point Load Strength Index (I_s), which serves as an indicator of the rock's mechanical strength (Broch & Franklin, 1985). The strength index (I_s) is determined based on the applied fracture load, the spacing between the platen tips, and the width of the fracture surface (Franklin, 1985).

$$I_s = \frac{P}{{D_e}^2} = \frac{\pi \cdot P}{4 \cdot W \cdot D} \tag{3}$$

Where:
I_s Point Load Strength Index (MPa or MN/m^2)
P is failure load in Newton (N)
D_e is equivalent diameter (mm)
D is specimen thickness (mm)
W is specimen width (mm)

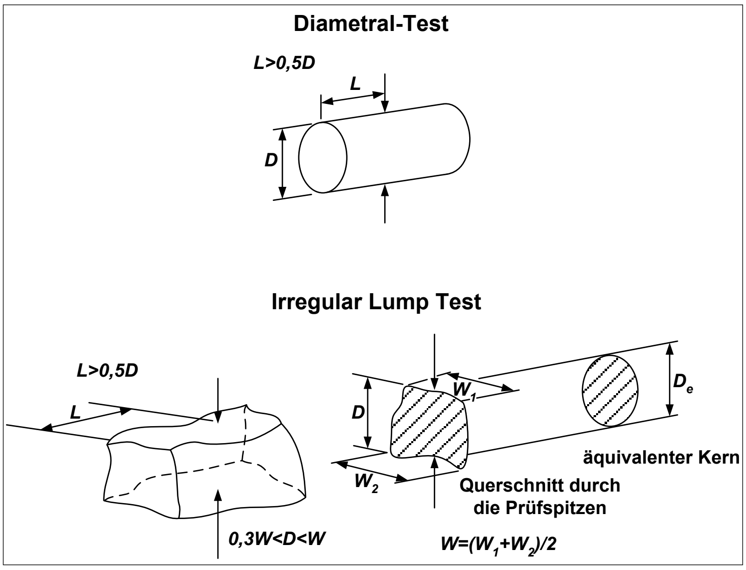

Figure 22: Specimens in Point Load Test (Franklin, 1985)

For the purpose of performing a regression analysis of measurement data on a logarithmic scale, Brook and the ISRM (International Society for Rock Mechanics and Rock Engineering) recommend applying a grain size correction factor f (Franklin, 1985; Brook, 1985). This factor allows for the standardization of the Point Load Strength Index to a reference diameter of 50 mm, denoted as $I_{s(50)}$. The corrected index is calculated as in Eq. (4):

$$I_{s(50)} = f \cdot \frac{P}{{D_e}^2} = \frac{P}{{D_e}^2} \cdot \left(\frac{D_e}{50}\right)^{2(1-m)} \tag{4}$$

Where:

m is the slope constant of the regression curve.

Since an empirical relationship exists between the corrected point load index $I_{s(50)}$ and the uniaxial compressive strength σ_D, the compressive strength can be approximated by multiplying $I_{s(50)}$) with a conversion factor c:

$$\sigma_D = c \cdot I_{s(50)} \tag{5}$$

According to ISRM guidelines (Franklin, 1985), the typical range for the ratio σ_D/ $I_{s(50)}$ lies between 20 and 25. Besides the strength index $I_{s(50)}$, which provides insights into the rock's compressive strength and thus its fracture and comminution behavior, the coefficient of variation is a valuable parameter for assessing the homogeneity of rock fragments in terms of their structure, texture, and mineral composition (Popov, 2007).

In this study, the mechanical strength of lithium-bearing ores was evaluated using the Point Load Test, applied to irregular lump samples representing four lithological categories: zinnwaldite mica-rich, zinnwaldite mica-poor, lepidolite mica-rich, and lepidolite mica-poor (Figure 23). Each sample is tested using a point load device to obtain a range of strength values representative of each material type. For statistical reliability, 20 to 30 measurements were performed for each lithological category.

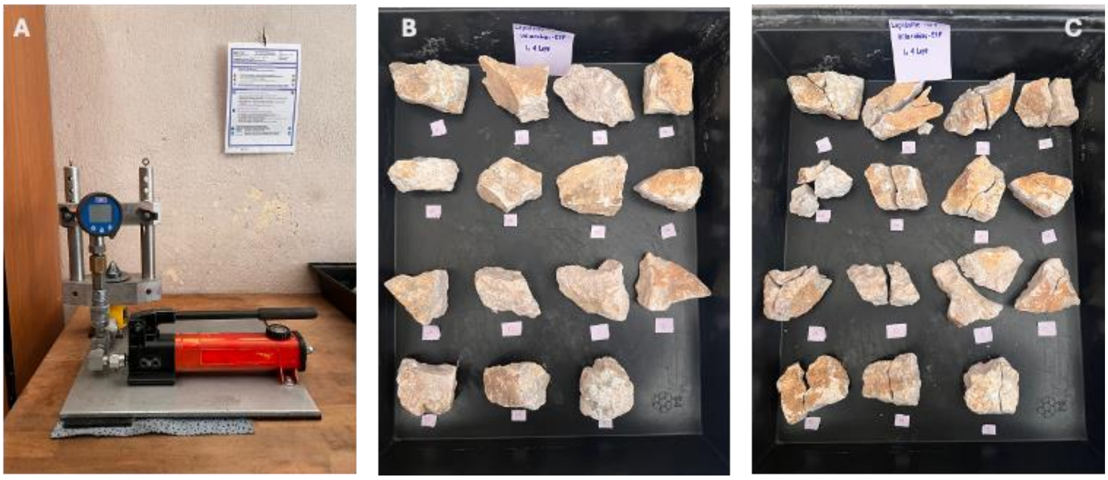

Figure 23: a) Point Load Test device b) Lepidolite samples before and c) After the breakage.

Testing was carried out using a portable point load tester from WILLE Geotechnik with a measurement range of 0 to 250 bar was used. The testing apparatus consists of a rigid steel frame, a manual hydraulic loading system, and a pressure gauge to record the peak load at failure. During testing, irregular rock samples are positioned between two conical steel plates, and the load is gradually applied using a hand-operated pump until the sample fractures. After failure, the dimensions of the fractured plane are measured. These measurements, together with the recorded failure load, are used to calculate the Point Load Strength Index $I_{s(50)}$. This index is used to classify rock strength and to estimate the Uniaxial Compressive Strength (UCS, σ_D), through empirical correlations. These mechanical strength values provide insight into the breakage behavior and comminution response of different lithium ore types.

Point Load Test Results

The zinnwaldite mica-rich greisen (GCG-1) and petalite ores exhibited the lowest strength, with an average $I_{S(50)}$ of about 2 MPa and a UCS of 53 MPa respectively. The zinnwaldite mix and zinnwaldite mica-poor (GCW-1) followed with $I_{S(50)}$ values of 2.85 MPa and 4.10 MPa, and UCS values of 71.3 MPa and 102.5 MPa, respectively (Figure 24, Table 7**¡Error! No se encuentra el origen de la referencia.**). According to ISRM classification (Table 8), GCG falls within the “moderate strength” range, while GCW is classified as “high strength.”

Table 7

Rock type	**$I_{S(50)}$, MPa**	**Standard Deviation**	**σ_D, MPa**	**Standard Deviation**
Zinnwaldite-Mix	2.85	1.13	71.3	18.2
Zinnwaldite-High Grade (GCG-1)	2.15	0.80	53.8	12.8
Zinnwaldite-Low Grade (GCW-1)	4.10	1.46	102.5	23.3
Lepidolite-Mix	4.75	1.62	118.8	26.0
Lepidolite-High Grade (LSR-1)	5.13	1.32	128.2	21.21
Lepidolite-Low Grade (LSA-1)	4.59	1.65	114.7	26.41

Petalite mix	2.00	1.08	50.0	17.24

Table 7: Point Load Test zinnwaldite, lepidolite and petalite ores, with conversion factor c=25

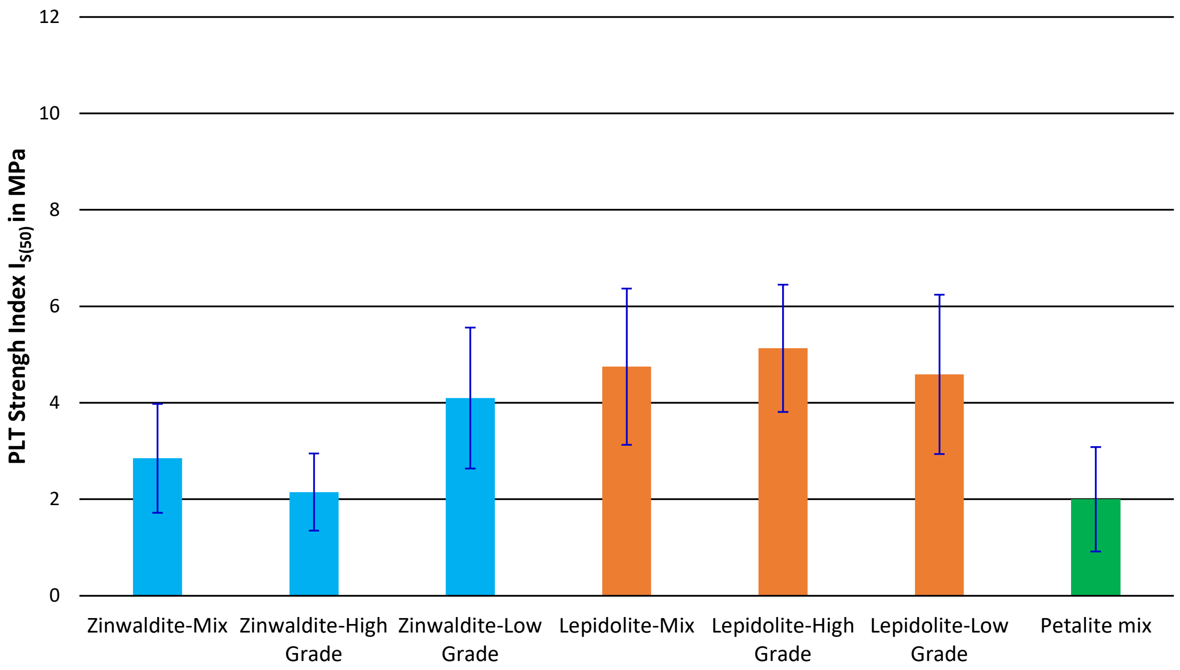

Figure 24: Point load test graph zinnwaldite, lepidolite and petalite ores

Geological Society		ISRM	
Description	UCS (MPa)	Description	UCS (MPa)
Very weak	<1.25	Very low	<6
Weak	1.25–5.00	Low	6–10
Moderately weak	5.00–15.50	Moderate	20–60
Moderately strong	12.50–50	High	60–200
Strong	50–100	Very high	Over 200
Very strong	100–200		
Extremely strong	Over 200		

ISRM (International Society for Rock Mechanics)

Table 8: Grades of unconfined compressive strength (ISRM..., 1981; The description...1977)

In contrast, lepidolite-bearing rocks showed consistently higher mechanical strength. The feldspar-lepidolite pegmatite (LSR-1 sample) recorded the highest UCS at 128.2 MPa, with an $I_{S(50)}$ of 5.13 MPa, followed closely by the lepidolite mix and lepidolite-poor aplite (LSA-1 sample), which showed UCS values of 118.8 MPa and 114.7 MPa, and $I_{S(50)}$ values of 4.75 MPa and 4.59 MPa, respectively. The low variation (16.1% in lepidolite mica-rich reflects a more homogeneous structure, suggesting consistent grain bonding. These rocks are all classified as “high strength” by ISRM and “very strong” by the Geological Society classification (Table 8).

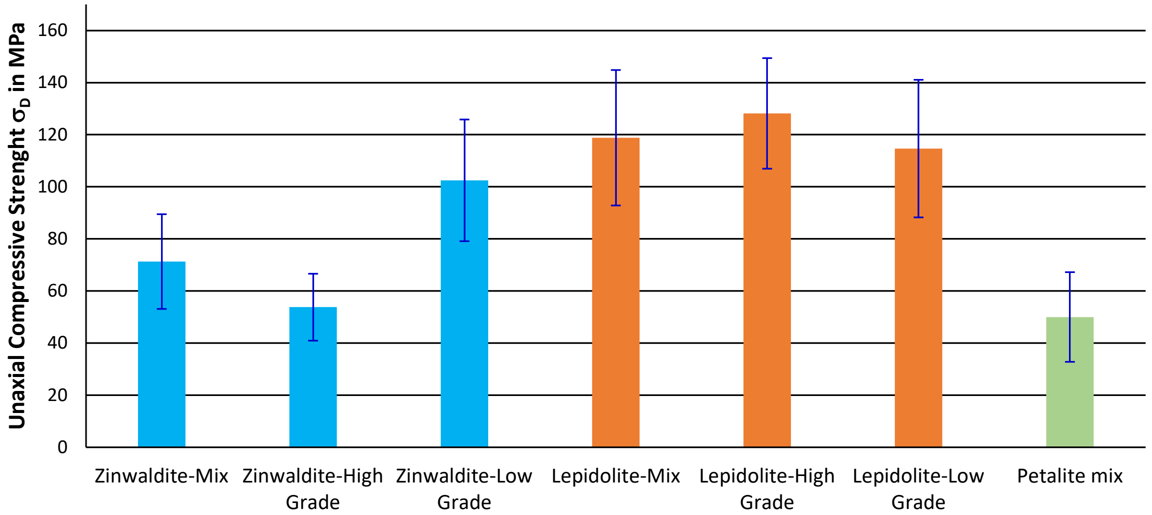

Figure 25: Uniaxial Compressive Strength graph of zinnwaldite, lepidolite and petalite ores

The zinnwaldite mica-rich greisen (GCG-1 sample) showed a significantly lower Point Load Strength Index compared to the zinnwaldite mica-poor greisenised granite (GCW-1 sample), despite the fact that the quartz content in the GCG sample is nearly twice as high. This counterintuitive result can be attributed to differences in microstructural features, particularly surface roughness and textural bonding, as identified through QMA analysis. The overall degree of roughness in the mica-rich zinnwaldite rock was measured at approximately 45%, whereas the mica-poor GCW sample exhibited a higher roughness value of around 60%, indicating more stronger interlocking between mineral phases. The low strength of zinnwaldite-rich greisen indicate that it is more susceptible to early breakage under mechanical stress.
Specifically, quartz crystals in the GCW sample displayed a roughness of up to 63%, compared to 45% in the GCG sample. As shown in thin section micrograph (Figure 26 b), the GCW is characterized by abundant microcrystalline quartz, which likely formed through recrystallization during greisenisation or hydrothermal alteration. This recrystallization enhanced the bonding between microcrystalline quartz and surrounding minerals, contributing to greater internal cohesion and mechanical strength. In contrast, the GCG sample is dominated by larger quartz crystals embedded in a relatively less altered matrix, resulting in reduced intergrowth and lower textural resistance to fracturing under point loading (**¡Error! No se encuentra el origen de la referencia.**a).

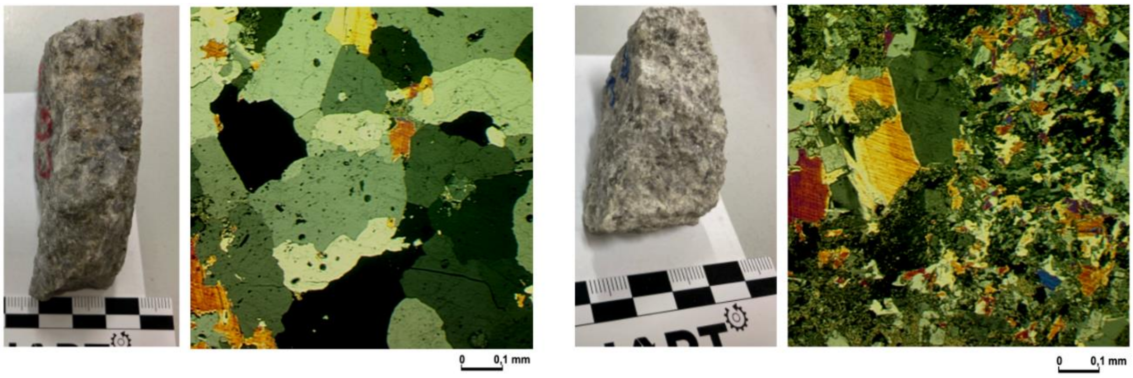

Figure 26: a) Zinnwaldite mica-rich (GCG) sample shows larger quartz crystal and less altered matrix. b) Zinnwaldite mica-poor (GCW) shows microcystallin quartz as predominant mineral in the altered matrix. 16x magnification thin section images.

The comparative results indicate that zinnwaldite ores, particularly mica-rich greisens, are mechanically weaker and more susceptible to breakage, making them more favorable for early-stage mineral liberation during comminution compared to lepidolite ore. However, their high quartz content also contributes to higher abrasiveness, which can lead to increased equipment wear. In contrast, lepidolite ores are more competent, requiring higher comminution energy to achieve sufficient size reduction and liberation. This increased resistance poses a higher risk of overgrinding, particularly given their finer grain size and more cohesive mineral textures, as observed in prior QMA analysis.

CONCLUSIONS

This study investigates the comminution behaviour and beneficiation potential of lithium-bearing ores, zinnwaldite from Cínovec (Germany-Czech border), lepidolite from Villasrubias (Spain), and petalite from Presqueira (Spain) by integrating mineralogical observation, mechanical characterisation, and processing experiments. The research is motivated by Europe's need for secure lithium supply chains, where low-grade, fine-grained lithium micas in the hardrock ore present both potential strategic and processing challenges.

Quantitative Microstructural Analysis (QMA) revealed distinct differences in the textural and structural characteristics of the studied ores. Zinnwaldite-bearing rocks (GCW-1 and GCG-1) are coarser-grained (mica: 0.7–1.3 mm) with high interlocking and roughness (KR up to 71%), while lepidolite-bearing sample (LSA-1 and LSR-1) showed finer grains (mica 0.1–0.2 mm), lower roughness, and more disseminated mica distribution indicated by its low clustering degree. These features influenced the breakage behaviour observed during mechanical testing and comminution.

In terms of mechanical characterization, zinnwaldite-rich greisen (GCG) and petalite ore have the lowest compressive strength (UCS = 53.8 MPa, Is(50) = 2.15 MPa and UCS = 50.0 MPa, Is(50) = 2.0 MPa respectively), while lepidolite-rich samples (LSR) recorded the highest UCS (128.2 MPa), attributed to their finer grain size and more cohesive structure. This suggests that lepidolite may require higher energy input and finer crushing stages to achieve target liberation size. Vickers microhardness confirmed that mica is mechanically weakest (154–195 N/mm^2) and ductile, whereas quartz and feldspar were much harder (>1200 N/mm^2) and tougher (KIC >2.0 $MN \cdot m^{-30.5}$). These mechanical contrasts from minerals are essential for enabling selective comminution, separate mica from gangue. Petalite has a moderate Vickers microhardness 611–1199 N/mm^2 and fracture toughness (0.78–3.2 $MN \cdot m^{-3/2}$).

REFERENCES

Popov, O. Beitrag zur mathematisch-petrographischen Gefügecharakterisierung für die Beurteilung der Festgesteine hinsichtlich ihrer Aufbereitung und ihrer Produkteigenschaften. *Dissertation*, TU Bergakademie Freiberg. 2007

Gurland, J. A study of contact and contiguitz of dispersion in opaque samples. *Trans. Met. Soc. AIME*, Vol. 236, S. 642-646. 1966

Burisch, M., Leopardi, D., Guilcher, M., Šešulka, V., Dittrich, T. & Lehmann, B. Greisen-Hosted Lithium Resources of the Erzgebirge/Krušné Hory Province (Germany and Czech Republic). *Economic Geology*, vol. 120, no. 3, pp. 627–647. May 2025, DOI: 10.5382/econgeo.5136.

Seifert, T., Neßler, J. & Gutzmer, J. Mineral resources in a sustainable world Strategic metals: their sources, and ore-forming processes New Sn-W Potential at the Zinn-wald/Cínovec Deposit, Eastern Erzgebirge, Germany. Nancy, Aug. 2015. [Online]. Available: https://www.researchgate.net/publication/305280042

Llorens T. & Moro, M. C. Microlite and Tantalite in The LCT Granitic Pegmatites Of La Canalita, Navasfrias Sn-W District, Salamanca, Spain. *The Canadian Mineralogist*, vol. 48, no. 2, pp. 375–390. Apr. 2010. DOI: 10.3749/canmin.48.2.375.

Guijarro, R.L., Agreement to acquire an interest in a lithium project, Greenland Mineral LTD, Perth. Jul. 2022.

Roda-Robles, E. et al., Geology and mineralogy of Li mineralization in the Central Iberi-an Zone (Spain and Portugal). *Mineral Mag*, vol. 80, no. 1, pp. 103–126. Feb. 2016. DOI: 10.1180/minmag.2016.080.049.

Dittrich, T., Seifert, T., Schulz, B., Hagemann, S., Gerdes, A. & Pfänder, J. Archean Rare-Metal Pegmatites in Zimbabwe and Western Australia Geology and Metallogeny of Pollucite Mineralisations. *Springer*. 2020 https://doi.org/10.1007/978-3-030-10943-1

Roza Llera, A., Fuertes-Fuente, M., Cepedal, A. & Martin-Izard, A. Barren and Li–Sn–Ta Mineralized Pegmatites from NW Spain (Central Galicia): A Comparative Study of Their Mineralogy, Geochemistry, and Wallrock Metasomatism. *Minerals*, 9 (12) 739. 2019. DOI:10.3390/min9120739

Kuangdi, X. The ECPH Encyclopedia of Mining and Metallurgy. Singapore: *Springer* Nature Singapore. 2024. DOI: 10.1007/978-981-99-2086-0.

Quinn, G. D. & Bradt, R. C. On the Vickers Indentation Fracture Toughness Test. *J Am Ceram Soc*, vol. 90, no. 3, pp. 673–680. Mar. 2007. DOI: 10.1111/j.1551-2916.2006.01482.x

Moradkhani, A., Panahizadeh, V., & Hoseinpour, M. Indentation fracture resistance of brittle materials using irregular cracks: A review. *Heliyon*, vol. 9, no. 9, p. e19361. Sep. 2023. DOI: 10.1016/J.HELIYON.2023.E19361.

Schreiber, S. Beitrag zur quantitativen Gesteinscharakterisierung zur Beurteilung von Gesteinen hinsichtlich ihrer Festigkeiten. *PhD Dissertation*, TU Bergakademie Freiberg, Apr. 2018.

Anstis, G. R., Chantikul, P., Lawn, B. R. & Marshall, D. B. A Critical Evaluation of In-dentation Techniques for Measuring Fracture Toughness: I, Direct Crack

Measurements. *J Am Ceram Soc*, vol. 64, no. 9, pp. 533–538, Sep. 1981. DOI: 10.1111/j.1151-2916.1981.tb10320.x.
Hunger, A., Gunther, C., Gebhardt, A. & Rüssel, Ch. Young's moduli and microhardness of glass–ceramics in the system $MgO/Al_2O_3/TiO_2/ZrO_2/SiO_2$ containing quartz nanocrystals. *Materials Chemistry and Physics,* vol. 122 pp. 502–506. 2010. doi:10.1016/j.matchemphys.2010.03.034
Luo, Y., Qu, C. & Mauro, J. C. High toughness transparent glass-ceramics with petalite and β-spodumene solid solution as two major crystal phases. *J Am Ceram Soc*. 2022; 105: 6116–6127. DOI: 10.1111/jace.18590
Hesse, M., Popov, O. & Lieberwirth, H. Increasing efficiency by selective comminution," *Miner Eng*, vol. 103–104, pp. 112–126. Apr. 2017. DOI: 10.1016/j.mineng.2016.09.003.
Broch, E. & Franklin, J. A. The point load test. *Pergamon Press*, 1972. DOI: 10.1016/0148-9062(72)90030-7.
Franklin, J. A. Suggested method for determining point load strength. *International Journal of Rock Mechanics and Mining Sciences & Geomechanics Abstracts*, vol. 22, no. 2, pp. 51–60, Apr. 1985. DOI: 10.1016/0148-9062(85)92327-7.
Brook, N. The equivalent core diameter method of size and shape correction in point load testing. *International Journal of Rock Mechanics and Mining Sciences & Geomechanics Abstracts*, vol. 22, no. 2, pp. 61–70, Apr. 1985. DOI: 10.1016/0148-9062(85)92328-9.
ISRM Commission on the Classification of Rocks and Rock Masses. Basic geotechnical description of rock masses. *Int J Rock Mech Min Sci Geomech*, 1981.
Geological Society Group Working Party Engineering. The description of rock masses for engineering purposes. *Quarterly Journal of Engineering Geology*, vol. 10, no. 4, pp. 355–388, Nov. 1977. DOI: 10.1144/GSL.QJEG.1977.010.04.01.